Internal Structuring of Semiconductors with Ultrafast Lasers: Opening a Route to Three-Dimensional Silicon Photonics

David Grojo, Maxime Chambonneau, Shuting Lei, Alexandros Mouskeftaras, Olivier Utéza, Andong Wang

Internal structuring of semiconductors with ultrafast lasers: opening a route to three-dimensional silicon photonics

David Grojo, Maxime Chambonneau, Shuting Lei, Alexandros Mouskeftaras, Olivier Utéza, Andong Wang

Abstract Important challenges remain to achieve reliable three-dimensional laser writing inside semiconductors as important as silicon. Experiments show that nonlinear energy deposition with long infrared laser pulses can modify silicon internally. However, the level of controllability is extremely limited compared with the femtosecond laser nanostructuring regimes reported in transparent dielectrics. Recent efforts have concentrated on the specificities of the bulk silicon response to tightly-focused ultrashort pulses. The strong propagation nonlinearities inherent to narrow band-gap semiconductors limit the space-time laser energy localization and prevent in most cases material breakdown with the shortest pulses. This Chapter proposes an overview of this emerging topic and the practical solutions to this problem. It also discusses the potential of three-dimensional laser nanostructuring in narrow band-gap semiconductors to address applications in different fields. Among them, the first demonstrations of refractive index laser engineering in silicon open the perspective to move silicon photonics from two-dimensional systems to monolithic

David Grojo
Aix-Marseille Univ., CNRS, LP3 UMR7341, Marseille, France, e-mail: david.grojo@univ-amu.fr

Maxime Chambonneau
Institute of Applied Physics, Abbe Center of Photonics Friedrich Schiller University, Jena, Germany, e-mail: maxime.chambonneau@uni-jena.de

Shuting Lei
Department of Industrial and Manufacturing Systems Engineering, Kansas State University, Manhattan, Kansas, USA, e-mail: lei@ksu.edu

Alexandros Mouskeftaras
Aix-Marseille Univ., CNRS, LP3 UMR7341, Marseille, France, e-mail: alexandros.mouskeftaras@univ-amu.fr

Olivier Utéza
Aix-Marseille Univ., CNRS, LP3 UMR7341, Marseille, France, e-mail: olivier.uteza@univ-amu.fr

Andong Wang
Aix-Marseille Univ., CNRS, LP3 UMR7341, Marseille, France, e-mail: andong.wang@univ-amu.fr

three-dimensional architectures.

Keywords: Femtosecond laser, 3D writing, silicon, semiconductor, waveguide, refractive index, silicon photonics

1 Introduction

Focused to small focal spots, intense light pulses lead to local nonlinear energy deposition allowing the production of micro-modifications at arbitrary location inside transparent materials [1, 2, 3]. In a few decades, this has led to the emergence of an alternative to lithography for direct micro-fabrication and rapid prototyping of micro-systems [4, 5, 6, 7]. According to experiments in dielectrics described in chapter 21, there are actually three main types of modifications which can be achieved with femtosecond lasers [8, 9]. First, at low intensities (i.e., slightly above the threshold for permanent modification), repeated bond breaking by multiphoton ionization leads to structural changes [10], and uniform refractive index modification ($\Delta n \approx 10^{-3}$) which allows the fabrication of waveguides and photonic circuits [1, 2, 11, 12]. Second, with repeated irradiations at higher fluences, the modification generally becomes heterogeneous with the formation of defects (from excitons [13] to lattice distortions, and reorganization on a subwavelength scale [14]). In fused silica, this culminates with the formation of well-ordered planar nanogratings perpendicular to the laser polarization [15, 16] attracting considerable interest for advanced technologies including photonics [17, 18, 19, 20, 21, 22]. Third, when extremely tight focusing conditions are employed, the extraordinary space-time confinement of the interactions leads to pressure and temperature conditions that are not accessible with other techniques [23, 24]. This latter regime forms void channels for microfluidic applications [25, 26, 27]. A particular attention is also given to these microexplosions for the synthesis of new allotropes of solids with unusual physical properties, opening possibilities for future technologies [28]. The physics behind the access these extreme states in silicon is the subject of chapter 12.

Taken together, these possibilities in dielectrics allow addressing lab-on-a-chip applications where laser writing can combine different optical, mechanical and fluidic functionalities, while any required electronic functionality is added by other means (e.g., lithography) so far. For this reason it is today highly desirable to achieve ultrafast laser internal structuring not only in dielectrics but also in semiconductors—especially silicon—to provide the ability to write directly hybrid devices combining electronics and other functionalities [29]. Due to the band-gap difference between dielectrics and semiconductors, this requires to translate high-power laser experiments in the infrared for accessing the transparency region of narrow-gap materials, where nonlinear ionization processes (e.g., multiphoton ionization) similar to those in dielectrics [30] are predominant.

In this Chapter, we review the recent works in this direction thanks to the advent of new high-power laser sources emitting in the infrared (e.g., Er- or Tm-doped fiber lasers) and optical parametric amplifiers (OPA) that become routinely available in research laboratories. We examine experimental results with pulse durations ranging from 60 fs to 150 ns, wavelengths in the 1.03–2.4-μm range, and various set of control parameters which have been tentatively exploited to achieve high-precision modifications inside crystalline silicon (c-Si) and other semiconductors. We describe the major challenges that remain to demonstrate the same level of controllability as in dielectrics. While the underlying fundamental aspects of high-intensity interaction in semiconductors are today only partially understood from very recent investigations, we review the main physical mechanisms explaining that the only reported modifications under conventional configurations have been achieved in two-photon absorption regimes with pulses or pulse trains with apparent durations from several picoseconds [31, 32] to nanoseconds [33] or more. Producing modifications in silicon with femtosecond pulses is generally doomed to failure, unless unconventional and impractical focusing conditions are employed [34, 35, 36]. The common denominator for all these demonstrations is that they aim at limiting the strong prefocal interactions. We will show how this constitutes a key to achieve sufficient energy deposition for producing permanent micro-modification inside semiconductors. The most recent successes that will be discussed in this Chapter open new and exciting technological perspectives including direct laser writing applied to the rapidly growing field of *silicon photonics* and the advent of laser solutions to meet some of the challenges of future microelectronics.

2 Long-pulse induced internal modifications in semiconductors and applications

2.1 Nanosecond laser-induced modifications

The topic of laser-induced sub-surface modification in semiconductors was pioneered in 2006 by Ohmura *et al.* who demonstrated confined modifications in c-Si by using 150-ns pulses at the fundamental wavelength of a Nd:YAG laser (wavelength $\lambda = 1064$ nm; photon energy $E_{\mathrm{ph}} = hc/\lambda = 1.16$ eV) [37]. This wavelength is not sufficiently high to access the region of full transparency for Si (band gap $E_g = 1.12$ eV) and, thus, to the production of modifications at arbitrary depths. However, by tightly focusing the pulses at depths less than the penetration depth ($\delta = 1/\alpha \approx 100$ μm at 1064 nm [38]), sufficient intensity contrast could be obtained, in turn leading to high absorption (by thermal runaway from near band-edge absorption) and subsequent material melting in a localized region near the focus. To apprehend the local band-gap closure with progressive temperature rise, one can refer to Varshni's empirical expression [39] which leads to a band gap below 1 eV for a temperature of 600 K, far below the melting threshold of Si ($T_{\mathrm{melt}} = 1687$ K

[38]).

The emergence of high-power erbium-doped nanosecond lasers emitting at 1550 nm motivated recent successful studies in the two-photon absorption regime to initiate similar localized thermal runaway [33, 40, 41, 42]. For all these heat-driven experiments in the nanosecond regime, the precision is limited by thermal effects—especially, heat diffusion. Simulations of the temperature change [37, 40] as well as images of the modified material [43] show that the melting threshold of c-Si can be largely exceeded in regions with smallest dimensions on the order of tens of micrometers unless complex multi-beam configurations are used to force a nonlinear collapse of the writing beam [33]. However, as the modifications are governed by thermo-mechanical effects, they remain similar to those reported in the initial paper of Ohmura *et al.* [37]. The main advantage of two-photon absorption compared to linear absorption is the capacity it provides to deposit the laser energy at arbitrary depths inside silicon. As two-photon absorption depends on the square of the intensity, it remains confined in the focal region at any processing depth. Figure 1 shows modifications written at two different depths in a Si wafer [33] with a 1550-nm nanosecond laser, and illustrates the 3D capability of this laser writing method.

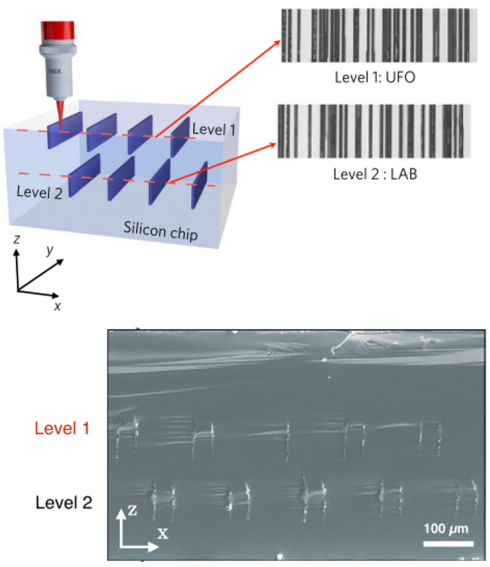

Fig. 1 Illustration of multilevel information data nanosecond laser writing and reading by infrared microscopy inside silicon (NA = 0.55, τ = 5 ns, E = 8 μJ). Bottom image is a cross-section of modification produced with the nanosecond pulses as observed by SEM. Level 1 and level 2 are respectively at 230 μm and 460 μm from the laser entrance side of the silicon wafer. Adapted with permission [33].

Nanosecond laser-produced sub-surface modifications consist of a melted volume that re-solidifies in more or less disordered regions that can take various allotropic forms (amorphous, polycrystalline or monocrystalline) [44]. For detailed analyses of the modified Si crystal structures, one can refer to the works from Verburg *et al.* [42] where transmission electron microscopy (TEM) and Raman spectroscopy were applied. The types of modifications that were found in different regions are: (i) perfectly re-solidified diamond cubic silicon with and without lattice defects, (ii) amorphous material, (iii) cracks, voids [45], and (iv) Si-III/Si-XII phases evidencing high-pressure conditions [46].

By means of infrared quantitative-phase microscopy, Li *et al.* investigated the refractive index change associated to these transformations depending on the applied laser conditions [43]. Consistent with the above-mentioned material analyses, this diagnostic revealed in most cases non-uniform modified zones with coexisting positive and negative refractive index changes. The index variations are reasonably associated to the creation of micro-cavities/porosities and densified regions. The overall apparent index variation is negative due to the important contribution of disruptions and porosities ($n \approx 1$) to the index change [33, 47]. Nevertheless, a study on channel writing [48] revealed interestingly it exist an appropriate scanning speed for which the melted material can redistribute advantageously to achieve a nearly uniform positive index change, as shown in Figure 2(b). As shown below, this positive- and negative-tone writing ability depending on the irradiation parameters with the same laser is today largely exploited for technological demonstrations.

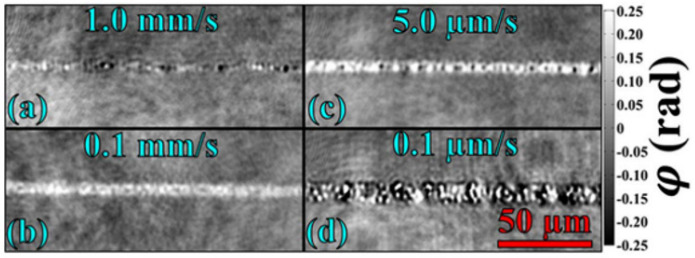

Fig. 2 Phase images of lines inscribed longitudinally inside silicon at different scanning speeds (NA = 0.45, τ = 5 ns, E = 2 μJ). The images reveal regions of positive (bright) and negative (dark) refractive index changes. Reprinted with permission from [48]©The Optical Society.

.

2.2 Potential applications

The first laser writing applications inside silicon relied on nanosecond pulses. Hereafter, we present various patented technologies and growing efforts to demonstrate

a level of control relevant for the fabrication of photonic microdevices.

Wafer dicing. A major successful application of sub-surface modifications by nanosecond lasers is wafer dicing by experimental developments based on the so-called *Stealth dicing* technology originally patented by the Japanese company Hamamatsu [49]. It consists of a two-step method where nanosecond laser pulses are first focused inside the wafer, which results in sub-surface modifications along lines inside the wafer. After laser processing, an external force is applied to the wafer which then cleaves the sample along the planes containing the subsurface modifications, thereby separating the wafer into individual chips. This method is especially valuable for the separation of sensitive devices such as microelectromechanical systems (MEMS), as it is dry and debris-free [50] in comparison to conventional laser ablation methods.

Data inscription. Another general application is wafer marking [51] or permanent data encoding in semiconductors [52]. In the example shown in Figure 1, Tokel et *al.* inscribed barcodes buried at different depths inside Si wafers and have demonstrated the possible reading of each independent layer thanks to infrared Optical Coherence Tomography (OCT) [52]. The method is attractive for the semiconductor industry because it is again surface-damage free, fast and does not damage surface area of the wafer on which are fabricated the integrated circuits.

Fabrication of waveguides and photonic microdevices. The possibility to control the refractive index of silicon with nanosecond laser pulses makes them attractive for directly integrating various optical functionalities in microelectronics wafers. An important subject is waveguide writing. In 2016, Chambonneau *et al.* demonstrated the possibility to inscribe longitudinal lines (i.e., along the optical axis) inside the material [48]. As shown by the phase images in Figure 2, the optical properties of the written lines strongly depend on the writing speed. For too high ($\geq$ 1.0 mm s^{-1}) and too low speed ($\leq$ 5.0 µm s^{-1}), the lines consist of a mixture between positive and negative index change, which is ascribable to the single-pulse configuration and cumulative effects, respectively. Interestingly, for 0.1-mm s^{-1} writing speed, the lines exhibit solely a positive index change $\Delta n = 5.3 \times 10^{-3}$ (assuming a cylindrical symmetry). These structures represent the first laser inscription of waveguides deep inside monolithic crystalline silicon, as confirmed by light injection in the structures. The same group has proposed strategies for optimized writing process for the fabrication of waveguides, gratings [53] and Y-splitters [54]. Process optimizations include the implementation of equivalents of the slit beam shaping technique for transverse writing [54]. In a recent work, Wang *et al.* first exploited transverse writing thanks to astigmatic beam shaping with a cylindrical telescope and a slit [55]. With this configuration, the authors demonstrated centimeter-long straight and curved waveguides inside silicon as shown in Figure 3. Power measurements showed losses around 3.3 dB cm^{-1} [56].

Besides the regime of gradient-index (GRIN) waveguide writing, the laser-produced modifications generally show a negative index change which can also

be advantageously exploited in this context. A remarkable illustration is depressed-cladding waveguides, as demonstrated by Tokel *et al.* [33], followed by Turnali *et al.* [47]. They created tubular modifications exhibiting a refractive index change $\Delta n = -3.0\times10^{-4}$. Despite the leaky nature of the guiding structures, excellent performance were reported since the losses were measured to be as low as $\alpha = 1.4\,\mathrm{dB\,cm^{-1}}$. By exploiting this negative index change, the authors not only demonstrated waveguides but also a large panel of optical functionalities including the inscription of Fresnel zone plates (lenses) and holograms [33].

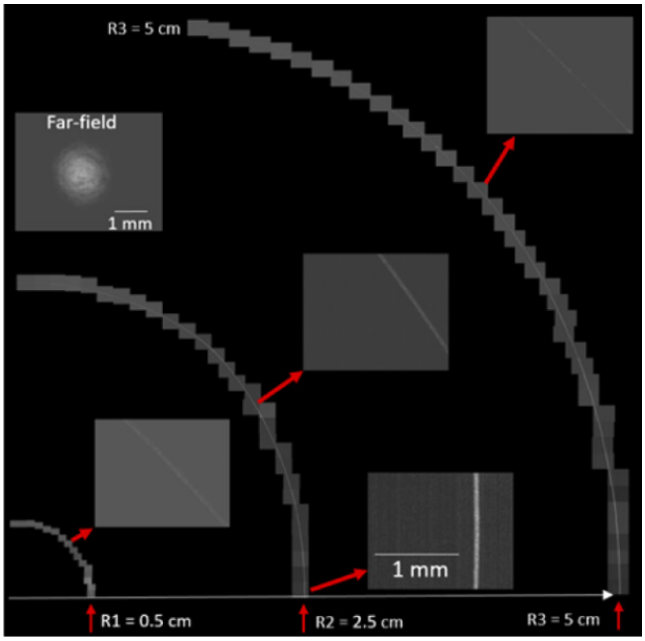

Fig. 3 Curved waveguides with different radii written transversely inside a Si wafer with a nanosecond laser. (NA = 0.85, astigmatically shaped beam, $\tau = 3.5$ ns, $E < 20\ \mu$J). Infrared light is coupled into each guide from the bottom of the figure shown by the red vertical arrows. The light scatters as it travels along a waveguide arc and this scattered light is imaged with an infrared camera. Top left image is the far-field light intensity distribution from the curved waveguide (2.5-cm radius). Reprinted with permission from [56] ©The Optical Society.

Femtosecond Laser Irradiation and Chemical Etching (FLICE). As nanosecond laser pulses can induce both positive and negative index change, works have demonstrated increased and decreased etching rates for the modified zone as shown with standard potassium hydroxide (KOH) anisotropic etchant for silicon in a recent work [57]. Noteworthy, this holds also for isotropic structuring with hydrofluoric acid (HF) allowing to reach an extremely high etching contrast for negative-tone structuring based on nanosecond laser-produced porosities. This was impressively exploited by Tokel *et al.* [33] with a plethora of complex structures demonstrated with this

method. A major achievement is, for instance, the creation of millimeter-long microfluidic channels inside silicon. Such channels constitute an interesting alternative to standard technologies employed for cooling microelectronic devices (e.g., microprocessors), with direct applications for increasing the clock rates [58].

All these experimental demonstrations concentrate almost exclusively on c-Si due to its technological importance but it makes no doubt that nanosecond laser subsurface modifications can be extended to any band-gap material (including the various semiconductors exploited by the microelectronic industry) provided that the wavelength is scaled properly with respect to the band gap. However, despite these important developments, the process performance should be improved for a transfer to high-precision applications. An illustration is *Silicon Photonics* that relies today on Silicon-On-Insulator (SOI) lithographic fabrication of circuits [59, 60, 61] exhibiting losses which can be as low as 0.1 dB cm^{-1}, and, thus, much lower than the above-summarized results. In particular, the large heat-affected zone associated with the modifications produced in the nanosecond regime will not reasonably allow one to demonstrate the same level of control as in dielectrics with femtosecond lasers. For this reason, ultrafast laser-produced modifications inside silicon using long-wavelength ultrashort pulses remain a natural option for the most demanding applications (resolution, quality, ...). However, it requires certain limitations to be circumvented as described in the following sections.

3 Ultrashort-pulse induced microplasma formation inside silicon and limitations

3.1 Qualitative picture and theoretical considerations

The nonlinear propagation and energy deposition of intense femtosecond laser beams in dielectrics is a subject of wide investigation for a few decades. In this Chapter, we do not intend to repeat the details of theoretical treatments that are described in chapter 1 of this book or in the literature [3, 62, 63]. However, we would like to highlight here that femtosecond interactions in semiconductors can be expressed with the same set of physical equations usually coupled through the nonlinear Schrödinger equation (under several assumptions) for the description of propagation accounting for diffraction, Kerr effect, group velocity dispersion, and nonlinear ionization with the associated plasma effects [64, 65]. However, a difference is the strong change in the magnitude and the relative importance of the contributing effects. The modified interplay leads to novel nonlinear interaction situations and new observations. As it will be developed below, it is also directly at the origin of the limitations which prevent, in most cases, to reach ultrafast breakdown conditions inside semiconductors [66, 67, 36].

To illustrate the deviation from dielectric studies, we summarize in Table 1 the typical values of some important physical parameters for fused silica (SiO_2), (i.e., the most widely studied dielectric material), and Si for comparison. Because most

Table 1 Important physical parameters for nonlinear interaction experiments in dielectrics and semiconductors. To illustrate the magnitude and relative importance of the different effects in both type of materials, we report the measured values found in the literature for SiO_2 and Si. For a direct comparison, these are sorted according to the multiphoton absorption (up to 4PA) regimes.

	units	Si	SiO_2	ratio	Ref.
Band gap E_g	eV	1.1	9		
2PA					
Wavelength window	nm	1200–2100	150–270		
Refractive index n_0		3.55–3.45	1.55–1.5	≈ 2.3	
Nonlinear refractive index n_2	$cm^2\ W^{-1}$	$\approx 7\times10^{-14}$	$\approx 5\times10^{-16}$	≈ 100	[68, 69]
Critical power for self-focusing P_c	W	$\approx 15\times10^{3}$	$\approx 8\times10^{5}$	≈ 0.02	
2PA coefficient $\beta^{(2)}$	$cm\ W^{-1}$	$\approx 1.5\times10^{-9}$	$\approx 1.7\times10^{-11}$	≈ 100	[68, 70]
Critical plasma density N_c	cm^{-3}	$\approx 6\times10^{20}$	$\approx 3.5\times10^{22}$	≈ 0.015	
3PA					
Wavelength window	nm	2300–3200	290–400		
Refractive index n_0		3.45–3.42	1.5–1.45	≈ 2.3	
Nonlinear refractive index n_2	$cm^2\ W^{-1}$	$\approx 7\times10^{-14}$	$\approx 3\times10^{-16}$	≈ 200	[71, 69]
Critical power for self-focusing P_c	W	$\approx 4.5\times10^{4}$	$\approx 4\times10^{5}$	≈ 0.01	
3PA coefficient $\beta^{(3)}$	$cm^3\ W^{-2}$	$\approx 2\times10^{-18}$	$\approx 10^{-23}$	$> 10^5$	[72, 73]
Critical plasma density N_c	cm^{-3}	$\approx 1.5\times10^{20}$	10^{22}	≈ 0.015	
4PA					
Wavelength window	nm	3400–4400	420–540		
Refractive index n_0		3.42	1.45	≈ 2.3	
Nonlinear refractive index n_2	$cm^2\ W^{-1}$	$\approx 3\times10^{-14}$	$\approx 2\times10^{-16}$	≈ 100	[71, 69]
Critical power for self-focusing P_c	W	$\approx 2\times10^{5}$	$\approx 10^{6}$	≈ 0.2	
4PA coefficient $\beta^{(4)}$	$cm^5\ W^{-3}$	$\approx 3.5\times10^{-31}$		> 100	[71]
Critical plasma density N_c	cm^{-3}	$\approx 0.8\times10^{20}$	5×10^{21}	≈ 0.015	

of these parameters are wavelength-dependent, we present a comparison at given multiphoton ionization orders $N_{ph} = \lceil E_g/\hbar\omega \rceil$ from 2 to 4. According to their respective band gaps (1.1 eV for Si and 9 eV for SiO_2) this leads to a comparison of the NIR/MIR domain for Si with that of the UV domain for SiO_2. We indicate the corresponding wavelength windows for which the measured values for each order are given. Because significant discrepancy can be found between measurements in the literature (especially for high-order multiphoton coefficients) we provide typical values for each considered window, a ratio between the values for Si and SiO_2 and the references from which the information has been extracted.

First, we note in Table 1 the high refractive index value intrinsic to narrow-gap semiconductors. As we will see later on, this causes a strong index mismatch at air-material interface limiting the achievable focusing conditions inside Si. We can also mention a somehow opposite situation in the time-domain for a comparison at a given multiphoton order. In contrary to UV for dielectrics, the NIR/MIR domain is in the near-zero group velocity dispersion (GVD) region for silicon. Therefore, we

do not expect significant complication as pulse stretching for situations in semiconductors [74]. When looking for the most important differences with the ratio column in Table 1, we note the much stronger nonlinearities in Si. Typically, a difference of two orders of magnitude in the nonlinear refractive index is observed. The associated critical power for self-focusing given by $P_c \approx 0.15\lambda_{las}^2/n_0 n_2$ for Gaussian beams is then on the order of a few MW for SiO_2, while it is only of a few tens of kW for Si. Considering a 100-fs pulse, this leads to the nanojoule energy level for interactions below the critical power inside Si. Similarly, we note orders of magnitude difference in the multiphoton absorption coefficients that results in increased absorption in the prefocal region for semiconductors. Also, because the critical plasma density N_c is inversely proportional to the square of the wavelength, the long wavelengths associated with multiphoton interactions in semiconductors lead to the occurrence of strong plasma effects (defocusing and absorption) at reduced carrier densities. These become important at typical free-carrier densities of 10^{21}–10^{22} cm^{-3} in dielectrics while they play a role at only 10^{20} cm^{-3} in femtosecond-laser-semiconductor interactions.

A conclusion is that the narrow gap of semiconductors associated to the long-wavelength required to reach multiphoton interactions lead to increased nonlinear propagation effects in comparison to dielectrics. This can be attractive for novel nonlinear propagation and filamentation-induced manipulations. However, it makes also more complex the achievement of controlled and highly concentrated energy deposition in the bulk of materials. Even under the tightest focusing conditions, nonlinear Kerr-induced phase distortions and strong plasma effects must occur in regimes where modifications would be expected in semiconductors. These aspects influence the controllability and complicate technological developments aiming at laser microengineering inside semiconductors.

3.2 Imaging experiments

The most direct method to study femtosecond laser-induced carrier excitation in transparent materials is ultrafast imaging using pump-probe optical setups [75, 76, 77]. Because dielectrics are transparent to visible light which can be sensed with standard Si-based detectors, various pump-probe methods were applied during the last decades for the measurement of all dynamical aspects from ionization, trapping of generated free carriers to material responses [78, 79, 75, 76, 77, 80, 13]. This metrology is progressively translated in the infrared to make possible similar measurements inside silicon and other narrow-gap semiconductors [66, 67, 81]. While obviously, the resolution limit decreases with the wavelength, using InGaAs array sensors and microscopy arrangements optimized at telecommunication wavelengths ($\approx$ 1300 nm or $\approx$ 1550 nm) allow one to reach enough precision to extract the free-carrier density and the size of the microplasmas created with tightly focused femtosecond pulses. Figure 4 shows an example of amplitude imaging of microplasmas created 1 mm below the surface of a c-Si sample by two-photon ionization with

90-fs 1300-nm pulses [81]. In practice, a beam splitter separates the beam in probe and pump pulses. The probe beam is directed to an optical delay stage and illuminates the Si sample perpendicular to the excitation by the pump pulse. By moving the delay stage, the optical path of the probe beam can be adjusted so the time difference between the pump pulse and the probe pulse is changed. The resulting images shown in Figure 4 represent the transmitted probe pulse, corrected for the background intensity measured without laser excitation. Interestingly, the high-mobility and long-lived characteristics of free carriers in Si combined to resolution-limited infrared imaging performances allowed one to observe directly the plasma expansion due to carrier diffusion [81] (which is hard to achieve in dielectrics due to the low mobility of carriers).

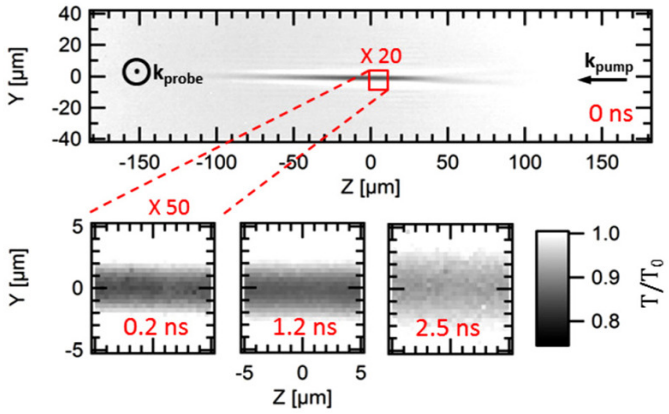

Fig. 4 Ultrafast infrared microscopy observation of a femtosecond laser-induced microplasma (E =20 nJ, NA = 0.3, λ = 1300 nm—2PA). The high-resolution images acquired for different delays reveal directly the expansion of the microplasma by free-carrier diffusion. Reprinted with permission [81].

To extract the free-carrier densities from the plasma linear transmission images, one can apply a Drude model accounting for inverse bremsstrahlung absorption of the probe. Both experimental works of Kononenko *et al.* [66] using high-energy focused pulses ($> 90\ \mu$J), and Mouskeftaras *et al.* for relatively tight focusing conditions (NA = 0.3) [67] conclude on sub-critical plasma densities in all tested femtosecond interactions in c-Si. They observed a clamping of the plasma density at a maximum level that is near or below 10^{20} cm^{-3}. This is significantly below the critical plasma density ($\approx 6\times10^{20}$ cm^{-3} at 1300 nm) and corresponds to absorbed energy density well below the melting point of Si (≈ 5 kJ cm^{-3}). A major difference with femtosecond-laser-dielectric interactions for which much higher absorbed energy densities have been reported [23, 24] is that ultrafast semiconductor interactions are inherently below the thresholds for material modification [36, 31]. The modest plasma density is also confirmed by the relatively long lifetime of the measured microplasmas ($\approx$ 2.5 ns) [81] as the decay of near-critical free-carrier densities should be on the

picosecond time scale, according to a dominant Auger recombination mechanism [82].

A major limitation of the technique lies in its sensitivity as the highest dynamic ranges of infrared cameras limit the minimum measurable absorption typically at levels of few percent (performance similar to standard Si-based technologies at best). In practice, this means that only densities exceeding 10^{17} cm^{-3} can be reasonably sensed for micrometer-size plasmas. To overcome this limitation, Wang *et al.* used luminescence microscopy to measure weak plasmas that are inaccessible with pump-probe method [83]. Their method relies on measurements of the photon emission from the plasma that has a very similar spectrum to what is expected from band-to-band radiative recombination after considering near-band edge absorption. Figure 5 shows the images of microplasmas created inside GaAs measured by both the luminescence and pump-probe methods. At low pulse energy of 0.4 nJ (τ = 190 fs, NA = 0.85), the luminescence image clearly detects locally created free-carriers while the pump-probe method fails. This clearly illustrates the advantage of luminescence microscopy for imaging low-density plasmas compared to the pump-probe method.

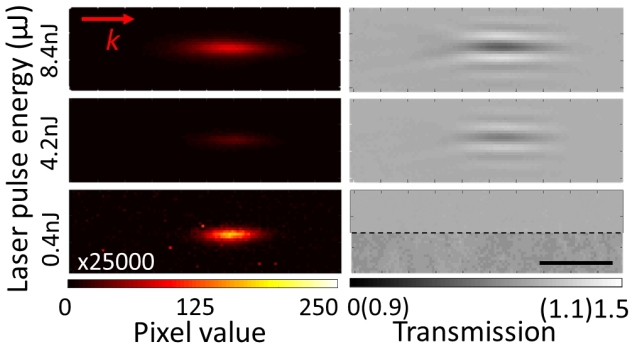

Fig. 5 Luminescence imaging compared to pump-probe shadowgraphy for observations of laser-induced plasmas inside GaAs. For the lowest pulse energy (0.4 nJ), the signal is magnified 25,000 times by increasing the exposure time and the digital gain. The scale bar of lower-half of the shadowgraphy image is rescaled between 0.9 and 1.1, showing no visible signal but only noise. The scale bar is 10 μm. The **k** vector marks the laser propagation direction. Reprinted with permission [83].

According to the recombination statistics in undoped semiconductors, the intensity of the luminescence is simply proportional to the square of the produced free-carrier density [84]. Accordingly, densities as low as $\approx$ 10^{16} cm^{-3} were retrieved by this method [83]. This is orders of magnitude lower than what is accessible with probe absorption methods [66, 67, 81]. Another benefit of the luminescence measurement is that it offers an incoherent imaging method that avoids diffraction artifacts as those visible in pump-probe images in Figure 5. This is of importance to

assess the details of spatial characteristics excitation in the 3D for situations which may be complicated by beam aberration and/or nonlinear propagation.

Beyond these imaging experiments, new infrared imaging developments will be needed to access more details of femtosecond-laser-semiconductor interactions. In particular, we anticipate that the advanced holographic imaging methodologies developed in the visible domain to study nonlinear interactions in dielectrics can be applied in the infrared domain [85, 80, 86]. It should allow one to retrieve not only the imaginary part of the refractive index with increased sensitivity but also the changes of its real part. These improvements are essential to follow both in time and 3D-space the dynamical aspects of ionization, as well as other effects such as the strong Kerr-induced nonlinearities described in the previous section which are inherent to narrow-gap materials.

3.3 Optical limitations to energy localization

There are different factors with strong interplays which contribute to the limitation of excitation by multiphoton ionization with femtosecond lasers in bulk semiconductors. Figure 6 summarizes those which have been clearly identified with the recent simulation and experimental works concentrating on c-Si but similar situations apply for the other narrow gap materials as confirmed by experiments turning to other semiconductors [83, 87].

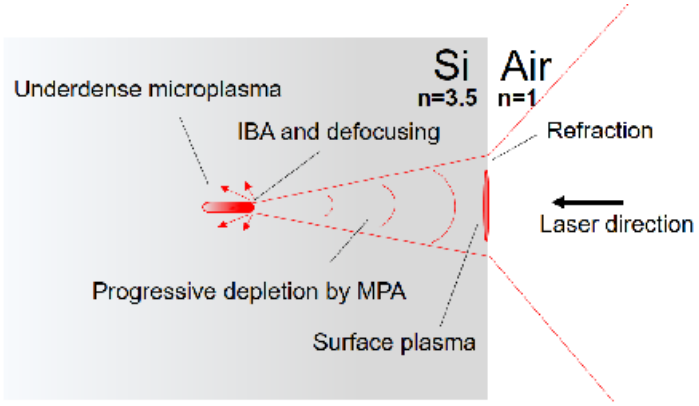

Fig. 6 Simplified schematic of physical effects identified as limiting the level of excitation by multiphoton ionization with femtosecond laser pulses in silicon. The strong refraction at the air-material interface leads to spherical aberration and near-paraxial propagation. The delivered intensity at the focus is limited by the progressive depletion due to highly efficient multiphoton absorption in the pre-focal region, inverse bremsstrahlung absorption (IBA) and defocusing of the underdense plasma which forms on front of the focus. When increasing the energy, a plasma will form at the surface, affecting the amplitude and the phase of the incoming focused beam until surface damage.

Focusing limitations. First limitations are related to the strong refraction that any beam focused in a high-index material will experience due to the strong index mismatch at the air-material interface. This will cause stronger spherical aberration than in dielectrics ($n \approx 1.5$), and will tend to lower the delivered peak intensity unless focusing optics specially designed to work in semiconductors are used [88]. Another direct consequence of the strong refraction is the relative paraxiality of beam propagation (modest focusing inside materials) even for experiments where beams are focused with high NA objectives. Taking a maximum of NA = 1 for an air-surrounded objective and a refractive index of $n = 3.5$ for Si, it is striking to note that the maximum half-angle of the focused beam inside the material (which is directly given by $\arcsin(\mathrm{NA}/n)$) will not exceed 16°. It is usually admitted that tight focusing leads to stronger confinements of integration limiting the importance of nonlinear propagation effects [4]. While this holds in dielectrics but it is not necessarily the case in some experiments in semiconductors. The strong nonlinearities (see above) combined with inherent paraxial propagation make that nonlinear effects can readily accumulate and transform the pulses before reaching the focus (see hereafter).

Pre-focal beam energy depletion. Another important effect that lowers the peak intensity at the focus is the progressive depletion of the beam by highly efficient multiphoton absorption in the prefocal region. To reveal the inefficient laser energy deposition caused by this effect, one can compare to the applied pump pulse energy E, the laser energy required to create the plasmas observed in ultrafast imaging experiments [66, 67, 81]. Assuming that each ionization event requires the absorption of two photons, a rough estimate is given by $E = 2\hbar\omega N_e V$ with N_e the free-carrier density, V the plasma volume [30, 88, 67]. Then, one observes that about 30% of femtosecond pulses of 10 nJ contribute to the ignition of the first microplasmas measurable by shadowgraphy [67] and the balance drops rapidly with progressive growth of a low-density plasma in the pre-focal region as directly evidenced by luminescence [83]. It reaches less than 1% for pulse energies of $\approx 100\ \mu$J [66] and so very modest energy densities are locally delivered in all conventional focusing cases.

Plasma defocusing/screening. The increased plasma effects associated with long-wavelengths add also a major limitation to bulk excitation. As near-critical plasma densities are approached (see pump-probe imaging described above) and/or significant effects are accumulated by propagation in a large pre-focal volume of low-density excitation (see luminescence imaging described above), the importance of inverse bremsstrahlung absorption and plasma defocusing [65, 66] progressively introduces more and more losses in the energy flux. This prevents from further feed any excited region behind a near-critical plasma front. A major difference between surface and bulk interactions is that increasing the pulse energy in the bulk moves the region of maximum plasma density in the backward direction [67] more than it enhances the maximum density produced [64, 36].

Nonlinear beam transformations. At high-energy levels, all the mentioned effects taken together will cause amplitude and phase distortions on the beam leading to important nonlinear beam transformations. Concerning these aspects, one can refer to the studies of Faccio *et al.* [89] and Kononenko *et al.* [90] both comparing

measurements with nonlinear propagation simulations. While these papers describe different situations, it is interesting to note that both groups reported a filamentation-like behavior with an elongated beam focus obtained by progressive transformation of the Gaussian profile into a Bessel-like profile with energy increase. To illustrate this aspect we show in Figure 7 the characterization of the fluence distribution of a femtosecond laser beam focused with a objective lens (NA = 0.42) at a depth of 1-mm inside c-Si. The procedure to retrieve the longitudinal fluence distribution (cross-section along the optical axis) is similar to that described in Ref. [91]. First, we note the similarity between the shape of the microplasma reported in Figure 4 and the fluence distribution measured for similar conditions (second image in Figure 7). As in previously cited reports [89, 90], a stretching along the optical axis of the fluence distribution according to a filamentation-like behavior is observed. Bessel-like beam profiles are also exhibited for energies exceeding 150 nJ. This adds a third observation (focusing with higher NA compared to previous cases [89, 90]) showing that the spontaneous beam transformation into a Bessel-like beam is likely a general feature of regimes of strong 2PA in semiconductors. This obviously does not help to deliver high-energy densities as the laser energy that is supposed to concentrate on the smallest possible spot spread progressively along the optical axis.

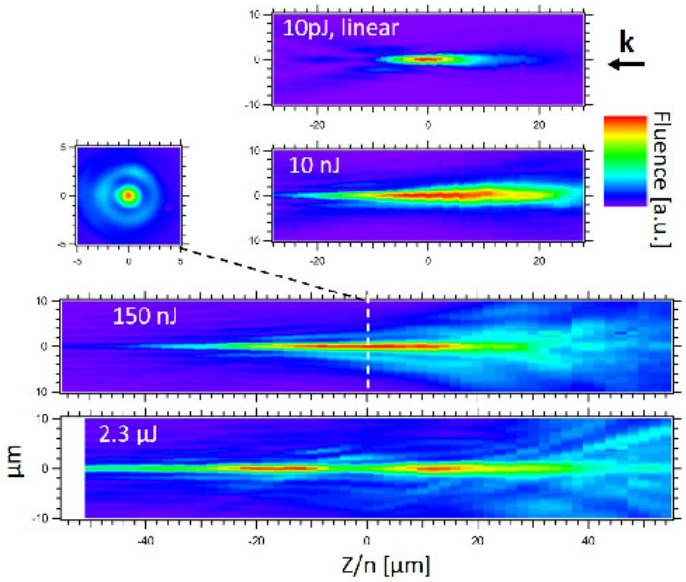

Fig. 7 Longitudinal fluence distributions at the focus inside silicon for increasing pulse energy (up to $E = 2.3\ \mu$J, $\lambda = 1300$ nm, $\tau = 100$ fs, NA = 0.42 and geometrical focus at a depth of 1 mm). When increasing the energy, the symmetry of low intensity Gaussian focus is rapidly broken due to plasma formation that prevents the pulse energy to pass through the geometrical focus. This is followed by a progressive transformation in a Bessel-like beam associated with a filamentation-like behavior for pulse energy at the micro-Joule level. Each fluence distribution is normalized to their respective maxima.

In the experiments, there is also a limit to the pulse energy that can be delivered for bulk processing and which is defined depending on the configuration by the fluence threshold for surface damage. The latter is on the order of 0.1–0.5 J cm^{-2} for regimes dominated by multiphoton absorption and pulse durations near 100-fs [92, 93] (note that this limit is obviously increasing with the NA and the depth at which the focus is placed inside the materials). At the highest energies below surface damage, high-density plasmas are formed on the surface. In this case [90], one can easily understand the transformation because one can draw a parallel with a well-known method to generate Bessel beams consisting of blocking the central portion of a spherical focusing lens [94, 91]. By conserving only the high-order angular components participating in the formation of the focus, a Bessel-like profile naturally forms by constructive interference along the optical axis. Here, the highly refractive and/or reflective plasma at near-critical plasma density acts as the element that prevents the central part of the beam to contribute to the focus and similar transformation are obtained. For energies that do not lead to the formation of surface plasmas, it is important to note that the transformations are observed at pulse energies exceeding by far the intensity level for measurable multiphoton absorption and the critical power for self-focusing. Then, the beam transformations rely on more complex nonlinear accumulated phase changes, absorption and diffraction in the bulk [89]. However, one can admit that most of the effects affect preferentially the central and most intense part of the beam leading to a similar transformation, as illustrated in Figure 7. The initial pulse energy of only 10 nJ that reveals already an elongated spot is one order of magnitude higher than the two-photon absorption threshold found under similar conditions [30]. Also, it is interesting to note that most of these experiments report filamentation responses but without catastrophic beam collapse despite beam power that can exceed by far the critical power for self-focusing. This can be attributed to the strong energy depletion lowering rapidly the apparent power as the beam propagate in the material discussed above. Another important remark on the discussion is also that most of the investigations have concentrated on spatial beam transformations but obviously the spectral and temporal characteristics of the pulses are also subject to important transformations in these situations [95, 96].

4 Strategies for enhanced ultrafast micro-excitation inside silicon

To overcome the limitations to the excitation, and to deliver sufficient intensity for femtosecond laser modification, different options have been investigated to date. They can be categorized in terms of optimizations of the interactions in the spectral, spatial and temporal domains.

4.1 Spectral optimizations up to the mid-infrared

An important remark that can be made on the comparison with dielectrics is that interactions at the fundamental wavelength of conventional femtosecond lasers lead to higher-order multiphoton absorption regimes compared to those tested in c-Si so far. For instance, the 800-nm wavelength (1.5 eV) of widely used Ti:Sapphire lasers leads to 6-photon absorption interactions in fused silica (band gap of 9 eV). However most of the investigations described here have been performed in the 2PA region of c-Si. This raises important questions: "*Is this difference in nonlinearity related to the limitations in energy densities that can be delivered in semiconductors?*", and: "*Can we increase the absorbed energy localization in c-Si with higher-order multiphoton interactions?*". This somehow revisits the question of a potential nonlinear resolution applied to in-volume studies, which is also a matter of debate for material surface processing [97].

In practice, femtosecond OPAs are today routinely available in laboratories and should allow to treat this question, but it is hard to repeat ultrafast laser experiments where the wavelength is the only changing parameter [98]. In addition, diagnostics get more complex for wavelengths outside the limited range of sensitivity of InGaAs sensors. In the literature, we find only few experimental studies on laser direct writing in bulk silicon that have been conducted with 3PA getting dominant at wavelength exceeding 2.1 μm [34, 30, 99]. All concluded about difficulties in achieving modifications inside Si very similar to what is reported in the two-photon regime. The work of Nejadmalayeri *et al.* [34] corresponds to the first attempt made for 3D writing inside silicon with a femtosecond laser. The modification produced at 2.4-μm wavelength could be only written in the subsurface of silicon at very limited depth through an interface with a cover glass. While this does not make possible a true-3D writing, it opens interestingly the perspective of a unique laser method for direct writing surface waveguides on silicon wafers. This potential alternative to SOI fabrication technologies was explored recently with pulses up the mid-IR in a recent work by Garcia-Lechuga *et al.* [93].

Interestingly, Zavedeev *et al.* [65] turned to numerical simulations to study the bulk interactions inside Si for wavelengths in a window from 1.2 μm to 5.25 μm (corresponding to regimes up to 5PA) in which the nonlinear coefficients of Si can be found in the literature [68, 100, 71, 101, 102, 72, 103]. Solving the nonlinear Schrödinger equation accounting for multiphoton absorption, optical Kerr and plasma effects under the paraxial approximation (NA = 0.3 considered), they found the counter-intuitive result that the maximum free carrier that can be achieved was decreasing when high-order multiphoton absorption comes into play. The results are illustrated in Figure 8, where the peak free-carrier density in the focal region is plotted as a function of wavelength (for 250-fs pulses of 500-nJ energy that is significantly above the requirement for a saturated delivered intensity in the 2PA regime [36]). A monotonous drop of the excitation down to densities below 10^{18} cm^{-3} is found at the exception of the spectral region exhibiting a peak in n_2 ($\approx$ 2 μm) which may provide Kerr-assistance for the focusing of the pulse. By looking at the space-time characteristics of energy delivery in details, the authors observed that the

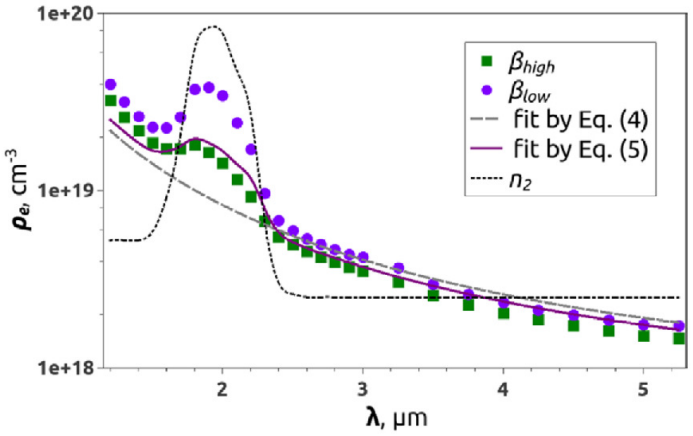

Fig. 8 Maximum free-carrier concentration at the focus, ρ_{max}, calculated inside Si as a function of wavelength (NA = 0.3). The calculations conclude on a monotonous decrease of the excitation density due to stronger plasma defocusing at increased wavelength. The calculations are performed for the highest and lowest multiphoton absorption coefficients found in the literature. The dashed line represents the wavelength dependence of the nonlinear refractive index (linear ordinate scale) which explains the local peak in the free-carrier density at the maximum Kerr-induced nonlinear focusing. Reprinted with permission [65].

prefocal depletion of the pulses reported for experiments at 1.3-μm wavelength [67] decreases significantly when increasing the wavelength. However, because plasma defocusing depends on the wavelength (according to Drude model for the permittivity) it actually takes over these prefocal effects near the focus. To simplify, one can easily apprehend that, without avalanche ionization which requires longer pulse duration to develop [88], it is difficult to expect the creation of a plasma density approaching the critical density in a nearly paraxial bulk interaction. Therefore, one could intuitively conclude that mid-infrared pulses are unfavourable for achieving breakdown conditions inside silicon. However, another and maybe more important quantity to consider for material modification is the deposited energy density. Rigorously, this adds the consideration of Joule heating of the free carriers in the energy balance. In contrast with the overall decrease in the electron density, the simulations revealed that the delivered energy reaches a minimum in the 3-photon absorption regime (at $\approx$ 2.8-μm wavelength), before growing in the 4- and 5-photon absorption regime. The benefit predicted in the mid-IR domain can be directly attributed to inverse bremsstrahlung absorption which is more efficient for long wavelengths but has not been confirmed so far by a successful bulk-Si writing experiment in this spectral region.

By taking all these aspects together a major conclusion is that longer wavelengths would make experiments more complex for a probably modest gain (if any) when aiming at ultrafast laser writing in bulk semiconductors. This likely explains why most experimental efforts have concentrated on optimisations in the spatial and temporal domains, as described hereafter.

4.2 Spatial optimizations up to extreme focusing

On the front of spatial optimizations, interactions inside c-Si with femtosecond micro-Bessel beams have been attempted as the propagation of such beams is known to strongly resist to nonlinear distortions. For Bessel beams, the energy flux is directed with a constant angle with respect to the optical axis (conical energy flux) which provides two advantages to deal with the previously listed limitations. First, it makes the interactions free from spherical aberration in comparison with tightly focused Gaussian beams which contain a wide range of angles of incidence [43, 104, 105]. Second, an even more important feature is that the intensity remains modest until the focus is reached. For high-Bessel angle, it is only here that significant nonlinear effects (including nonlinear beam distortions and nonlinear absorption) occur [106]. These beams therefore intrinsically lead to controlled interactions at higher intensities compared to Gaussian beams, and they have been already exploited for fabricating high-aspect-ratio nanochannels in glasses using single femtosecond pulses at 800-nm wavelength [26, 74].

High-angle femtosecond micro-Bessel beams ($> 20°$) [107] at 1300-nm wavelength have been produced by axicon-based methods and characterized to compare interactions in dielectrics and c-Si. Also, high-energy versions [74] of the beams leading to ultrahigh intensities ($> 10^{15}$ W cm^{-2}) over millimeter-long filaments have been tested. A direct comparison of the modifications induced in borosilicate glass and c-Si samples with micro-Bessel and focused Gaussian beams is shown in Figure 9. For glass, it is found that the Bessel beams produce complete through-hole modifications with an efficiency very similar to that of commonly used 800-nm wavelength pulses [108, 26, 109, 110]. However the response in c-Si is drastically different. We note that the surface damage threshold is largely exceeded. The stronger damage in comparison to glass are associated to the high two-photon absorption coefficient of Si. However, for both micro-Bessel and focused Gaussian beams there is no noticeable material modification in the bulk. In another experimental study, He *et al.* have evidenced the fabrication of high-quality through-silicon vias which constitute an essential building block for vertical electrical connections in 3D integrated electronics circuits using femtosecond Bessel-like beams at 1.5-μm wavelength [111]. The corresponding realizations were nevertheless obtained on ultra-thin wafers, and employing a percussion drilling technique with sequences of 1,200 high-energy (104 μJ) 65-fs duration pulses. Therefore, these conditions are radically different from single-shot drilling experiments in dielectrics.

An interesting complementary measurement achieved in these configurations is the one of the intensity delivered in the bulk which exhibits a clamping at $\approx 4 \times 10^{11}$ W cm^{-2} with $\approx$ 100-fs pulses [107]. The corresponding fluence (0.05 J cm^{-2}) is well below the typical thresholds for surface modification of silicon ($F_{\text{th}} > 0.1$ J cm^{-2}) [112, 92], but this intensity value exceeds significantly the level for measurable two-photon ionization ($\approx 10^{10}$ W cm^{-2} [30]). Then, we can derive from the measurement a rough estimate of the produced free-carrier density with the relation $N_{\text{max}} = (\tau\beta I_{\text{max}}^2)/(2\hbar\omega)$, where $\tau = 110$ fs, β and $\hbar\omega = 0.95$ eV are respectively, the pulse duration, the two-photon absorption coefficient and the pho-

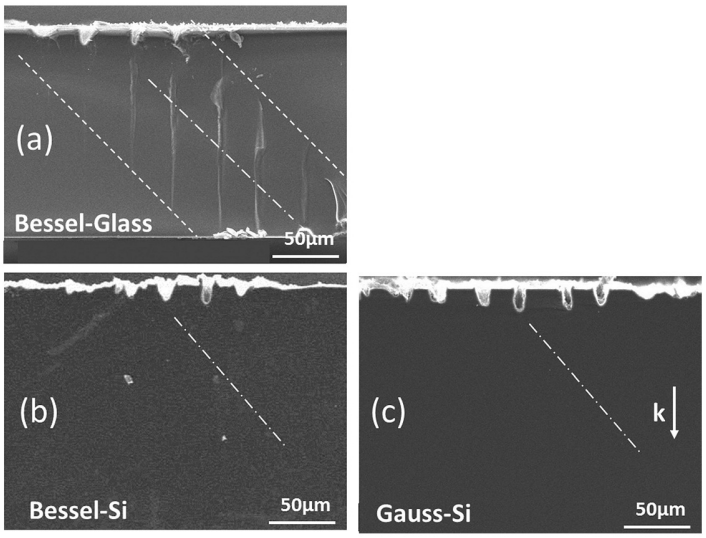

Fig. 9 Comparison between modifications induced in glass and silicon for a pulse energy of 12 μJ delivered on the target (τ = 100 fs, λ = 1300 nm—2PA). For all substrates, lines are written at different depths and cross-sections are observed with scanning electron microscopy (SEM). The material disruption induced by the Bessel beam in glass extends over the entire thickness (a) but remains confined at the front surface in Si. Similarly, there is no confined modification observed in the bulk when Gaussian focusing is applied (c). The dashed dotted line shows the evolution of focus position to guide the eyes. Reprinted with permission from Ref. [107]

ton energy. This relation assumes again the absence of collision-assisted ionization such as impact ionization leading to avalanche ionization [88]. Using a two-photon absorption coefficient [113, 68, 102] in the range of 0.5–1.5 cm/GW, we find a maximum free-carrier density $N_{\max} = 2.9\text{–}8.1 \times 10^{19}$ cm^{-3} which matches remarkably the value found with the measurements based on ultrafast imaging of the plasma created by Gaussian beams (see previous section). These considerations show that the benefit of Bessel beams on ultrafast Si excitation (if any) remains very modest in the tested situations. One possible reason for this limitation is that significant spatial improvement would require a large-angle cone of light (i.e., breaking the paraxiality). Unless more exotic beams as ring-Airy beams that exhibit a parabolic energy flux and nonlinear collapsing features [114, 115] are implemented, this will always remain particularly challenging due to refraction at the input interface of high-refractive-index semiconductors. Even if the Bessel beams that have been produced rely on high angles, they do not exceed the highest angle components in tightly focused Gaussian beam experiments.

The identified requirement of high angular components introduces the first methods that has lead to the production of modifications in bulk silicon with femtosecond laser pulses. It consists of employing hyper-NA configurations (i.e., numerical apertures well above unity) so that the energy is spread on the largest possible range of angular components and the intensity in the prefocal region is minimized. To do so,

Sreenivas *et al.* have employed an oil immersion microscope objective of numerical NA = 1.25 and index matching liquid of refractive index 1.49 for focusing in bulk silicon 800-fs duration laser pulses at 1.55-μm wavelength and a pulse energy of 50 μJ [35]. The authors reported on buried structures in the material, ascribable to the higher intensity at the focus together with large angles of the cone of light which limit detrimental prefocal nonlinear interactions. While this liquid immersion focusing surely improves the situation, important limitations persist due the limited refractive index that makes it difficult to perform experiment with effective NA > 1.5. To illustrate this aspect, it is interesting to note that the corresponding half-angle of the cone of light in Si is only 35° which remains modest in comparison to what is readily achieved in dielectrics. Therefore, the experiments show that this methodology is insufficient for achieving 3D writing with even-shorter pulses [36].

In order to solve this issue, Chanal *et al.* have proposed to implement the concept of the solid immersion lens (SIL) technique used in advanced in microscopy [116, 117] for a laser writing configuration [36]. As a proof-of-concept experiment, 60-fs laser pulses at 1.3-μm wavelength were focused in the center of a 2-mm diameter silicon sphere with objective lenses up to a numerical aperture of NA = 0.85. In this configuration schematically depicted in Figure 10, the wavefront of the beam matches the air-silicon interface, suppressing refraction. The effective numerical aperture of the laser writing experiment thus becomes the one of the objective lens multiplied by the refractive index of silicon $\mathrm{NA_{eff}} = n_{\mathrm{c\text{-}Si}} \times \mathrm{NA_{obj}} = 2.97$. Supported by nonlinear propagation simulations with the model developed in Ref. [64], these extreme focusing conditions produced the very first modifications in bulk silicon with < 100-fs duration pulses. The remarkably low pulse energy sufficient for producing these modifications (20 nJ) as well as the repeatability of experiments when changing the spherical sample confirmed that the laser-produced modifications did not rely on defects inside the material [118]. The refractive index change associated with the modifications is negative, suggesting that these consist of voids or micro-cavities in these tested conditions.

An important conclusion from this success is the absence of a strict physical limit which prevents modification with femtosecond pulses. The introduction of more angular components than those supported by conventional writing configurations provides a solution to circumvent the aforementioned limitations related to nonlinear propagation. However a practical implementation will remain challenging for wafer processing. This will require an astigmatic solid immersion lens (ASIL) made of silicon (e.g., less than a half-sphere) positioned on a wafer surface to produce modifications similar to those shown in Figure 10 inside the wafer. While such experiments have been successful for microscopy purposes [116, 117], there is no equivalent to date with a material writing beam.

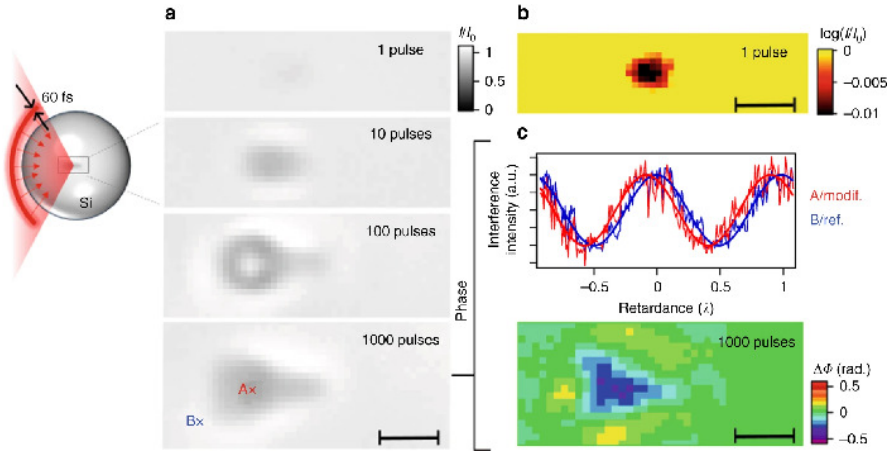

Fig. 10 Micro-modification produced in bulk silicon with 60-fs duration laser pulses through a spherical interface. (a) Bright-field images of the modifications for different number of applied pulses. (b) Transmission image of a modification induced by a single pulse in logarithmic scale. (c) Phase measurements of a modification induced by 1,000 pulses including (top) an interferogram comparing the phase on the two points A and B indicated in (a), and (bottom) a two-dimensional phase image. Laser wavelength: 1.3 μm; Pulse duration: 60 fs. Reprinted with permission from Ref. [36].

4.3 Temporal optimizations for practical writing solutions

We have introduced the capacity of nanosecond lasers to induce heat-driven damage in the bulk of semiconductors, and the relative harmlessness of ultrafast energy deposition. This likely indicates that optimizations of the temporal shape must be possible to achieve stronger energy deposition—and potentially improved controllability on 3D modifications. Several strategies have been proposed to optimize the pulse temporal shape for producing modifications inside silicon.

Picosecond regime. A first consideration is to explore the intermediate picosecond pulse duration that are as short as possible to keep the benefit of ultrafast energy deposition. To this end, several groups have investigated the modification inside Si by using picosecond pulses with variable pulse durations. Kämmer *et al.* showed that permanent modifications could be produced with infrared 0.8–10-ps pulses at 1.55 μm pulses [119]. However, the maximum damage probability of 95% measured for 10-ps pulses suggested that damage production could not be achieved in a deterministic and repeatable way. At the same wavelength, Das *et al.* further investigated the 4–21-ps regime for modifying bulk Si. Results in Fig. 11 show that a minimum duration of 5.4 ps is required to produce modifications. By employing pulses at the advantageous wavelength of 2 μm for increased energy deposition inside silicon [120], Chambonneau *et al.* showed that the pulse duration threshold for the production of repeatable modifications could be lowered to 2 ps [57]. Another interesting aspect related to picosecond-laser-produced modifications shown in the same study

is the non-monotonic evolution of the damage probability and the deposited fluence as a function of the input pulse energy [57]. Such an unusual behavior was measured for 2 ps pulses, but not for longer pulses (9 ps and 400 ps). This phenomenon was confirmed by Das *et al.*, as shown in Fig. 11, with a peak power upper limit (energy threshold) above which no damage is formed (Regime D in the map) [32]. These results indicate the persistence of strong nonlinear propagation effects delocalizing the radiation in the picosecond regime.

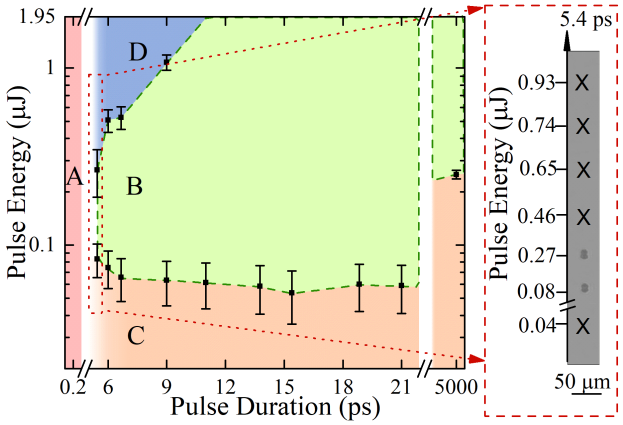

Fig. 11 Laser conditions for achieving micro-modification inside silicon with a 1550-nm wavelength laser pulses focused with NA = 0.85**.** The pulse energy and pulse duration ranges for modification with 100% probability are shown with region 'B' in green. The set of parameters leading to the absence of modifications are divided in 3 zones: 'A', the region where the pulse duration is too short to achieve modification independently of the pulse energy; 'C', a region below energy threshold for modification, and 'D', a region corresponding to high-power regimes where the energy deposition is strongly delocalized leading to local energy densities below the damage threshold. The inserted image (right part) shows the IR microscopy image of modified spots systematically irradiated with 1,000 pulses of 5.4-ps duration at different pulse energies where non-damaged parts are symbolized as cross marks. Reprinted with permission from [32] ©The Optical Society.

Multi-pulse optimizations. A second approach for temporal optimization is to use high-repetition-rate bursts. If the repetition rate is sufficiently high, accumulation of heat and/or free-carriers may lead to the production of permanent modifications. In this way, the energy of each sub-pulse can be much lower—thus avoiding the detrimental intensity clamping induced by high-energy unshaped pulses. Using this approach, Mori *et al.* and Shimotsuma *et al.* [121, 122] showed the first internal modifications in semiconductors by using femtosecond pulses trains consisting of two sub-pulses. By using a Cr:Forsterite amplified femtosecond laser system operating at 1.24-μm wavelength with 110-fs pulse duration, they first confirmed that it is impossible to induce any structural changes inside c-Si with repeated single-pulse irradiation despite high-energy pulses (600 μJ), and a large numerical aperture (NA = 0.85) for focusing. However, by repeatedly illuminating silicon with double-

pulse trains of ≈ 50-μJ energy, they successfully obtained embedded modifications taking the form of periodic nanostructures. Figure 12 shows an electron microscopy image of the modifications captured after polishing the irradiated samples down to the level necessary to have the modifications intercepting the surface. The motivation

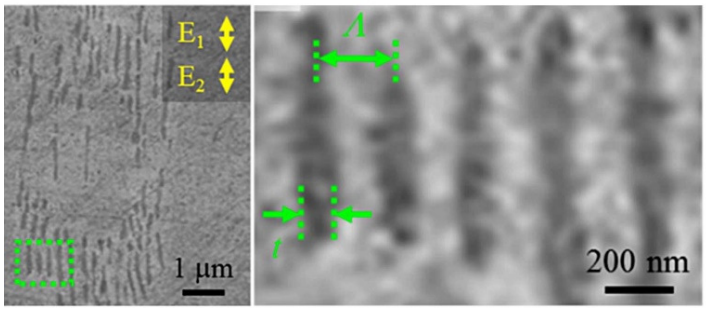

Fig. 12 Self-organized nanostructures formed inside c-Si by illumination with pulse trains of two femtosecond pulses. These are secondary electron (SEI) images of polished samples down to the depth of the focus position after laser irradiations with 1000 double-pulses of 120-fs duration, ≈ 25-μJ energy and delayed by ≈ 1 ps. and focused with NA = 0.85. Adapted with permission [121].

of applying double-pulses to deposit higher energy densities was directly inspired by a method applied in dielectrics to separate and control individually plasma ignition (first pulse) and energy deposition by free-carrier heating and avalanche (second pulse) [123, 124]. Accordingly, the reported modifications were obtained for pulse separations from 1 ps to 1 ns, which is the time scale without significant decay of free-carrier density in Si [81]. The authors found that an appropriate energy ratio between the two pulses is required so that the second arriving pulse can interact with a plasma of adequate density to avoid that most of the energy gets reflected or defocused. Typically, double-pulses (of 120 fs each) with equally-divided pulse energy were employed. This raises questions on the strongly different results obtained in comparison to previously performed experiments with twice longer pulses (250 fs) in which material modification was impossible [66]. This was only recently understood on the basis of the detailed contrast characteristics of the applied pulses [31] and discussed below.

Recently, Wang *et al.* generated THz-repetition-rate pulse trains by using a series of birefringent crystals with different thicknesses [125]. This extremely high repetition rate prevents from strong energy dissipation inside silicon between pulses. The situation illustrated in Figure 13(a) thus enables unique capabilities for accumulation of free-carriers generated by nonlinear ionization and heat causing progressive band-gap closure during the applied trains. Space-resolved measurements evidenced changes in the interplay between detrimental nonlinearities and accumulation effects depending on the number of pulses in the trains and a net increase in the level of achievable energy deposition was observed under appropriate conditions. The im-

provement was also supported by experiments demonstrating high performance for 3D laser writing inside silicon. As shown in Figure 13(b), irradiation with trains of only 4-ps pulses with the same total energy ($\approx 2\ \mu$J) leads to drastic improvements of the repeatability and the uniformity of the produced features in comparison to repeated single-pulse irradiations.

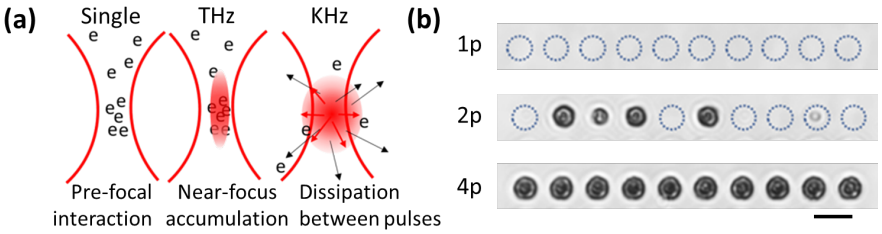

Fig. 13 Ultrafast laser writing inside Si with THz-repetition-rate trains of pulses. (a) Schematic representation of expected accumulation effects in Si. Single pulse irradiation leads to strong detrimental prefocal plasmas that prohibit modification. The same energy provided in a Terahertz burst irradiation lower the apparent intensity but heat and free-carrier accumulation between pulses can be expected. (b) Si-bulk writing experiment comparing the results of irradiation at a given energy with trains of 1, 2 and 4 picosecond pulses (NA = 0.85, E = 2.1 μJ, τ = 4.7ps). The irradiation are repeated 10 times. Higher delivered energy density is evidenced by progressive improvement of writing reliability when increasing the number of pulses in the trains. The scale bar is 20 μm. Adapted with permission [125]

Temporal characteristics of pulses and imperfections as drivers. In contradiction with most previous reports, some recent works conducted using fiber lasers have interestingly demonstrated successful waveguide writing inside Si with femtosecond pulses under conventional conditions [126, 127, 128]. While the authors mention sometimes the need for a local imperfection to seed the writing process, it tends to show however that more favorable conditions for writing can be found in these particular fiber laser experiments. For instance, Figure 11 shows the incapacity of achieving modification with pulses of durations < 4 ps using even higher NA than those used in these waveguide writing experiments. A main difference between the applied laser technologies as pointed out in a recent work is the temporal contrast of the pulses [31]. In an experiment consisting of irradiation of silicon with synchronized femtosecond, picosecond, and nanosecond pulses, Wang *et al.* could intentionally adjust the apparent temporal contrast of femtosecond irradiations [31]. Figure 14 shows a comparison of femtosecond laser modifications obtained while varying the contrast value with a picosecond pre-pulse. In agreement with previous studies relying on OPAs, these results confirm that highly contrasted femtosecond pulses are inoperative for writing. However, with degraded contrast, modifications can be produced. Interestingly, an optimum for low modification threshold is found at contrast value corresponding very well with those typical for fiber technologies. Overall, by multi-time scale analyses of these aspects (ps and ns contrast), this study

reveals a sensitivity to the temporal contrast at an unusually high level for laser material processing applications.

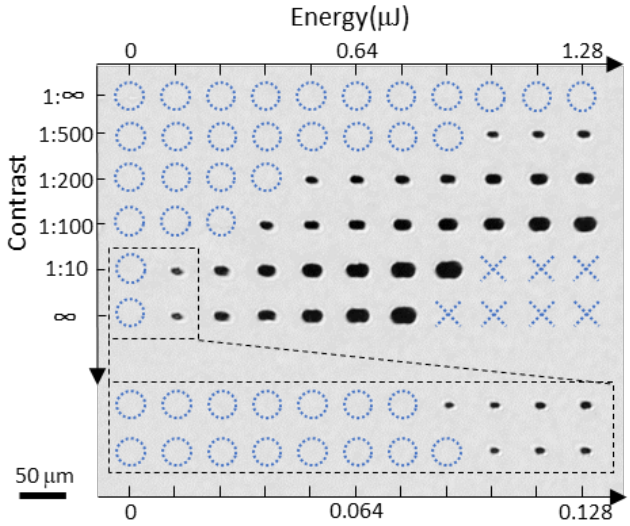

Fig. 14 Bulk Si modifications obtained after irradiation with 190-fs pulses and picosecond prepulse contrasts of different energies on separated sites. The duration of the prepulse degrading the contrast is 10 ps. The impacts are made 300 μm below the surface and observed with infrared microscopy. The blue circles indicates irradiations without modifications and crosses are cases in the matrix that have not been tested because of laser energy limitations. We note the incapacity of achieving modification with high-contrast femtosecond pulses and a contrast-dependent modification threshold given by the transition between the last circle and the first modification on each line. Reprinted with permission from Ref. [31]

These results on the influence of the temporal contrast have been also observed by Chambonneau *et al.* who have recently employed temporally distorted 750-fs pulses for achieving ultrafast transverse inscription in the bulk of silicon [105]. In this study, it was shown that repeatable modifications could not be produced with temporally bell-shaped pulses, even by using the beneficial wavelength of 2 μm (where the energy deposition is the highest [65]) in addition to a focus position for which spherical aberrations of different origins mutually balance. In stark contrast, utilizing temporally distorted pulses allows one to increase the energy deposition, leading to repeatable modifications which are the building blocks for transverse inscription. The morphology of the transversely written lines can be discrete, continuous, or erratic, and mainly depends on the writing speed, and also on the input pulse energy [105].

5 Emerging three-dimensional solutions for the semiconductor industry

5.1 Applications in microelectronics

In this Chapter, we describe the vision of laser writing contributing to the technological developments in *Silicon Photonics*. However, the associated index engineering applications will require an extremely high level of control of laser-induced transformations of silicon. This will need further fundamental and applied efforts for optimizations and can only be seen as a mid-term or long-term perspective. It remains that the recent knowledge in the field has lead to new approaches immediately applicable in the semiconductor industry.

Electrical control in silicon chips. As developed in previous sections, laser direct writing in bulk silicon with femtosecond pulses is extremely challenging. Nevertheless, the transient microplasmas—and thus, the induced current—inside silicon in a non-invasive way offers a range of other applications. Some applications are local electrical testing inside integrated circuits by laser. The carrier injection process namely photoelectric laser stimulation (PLS) can be synchronized with static or dynamic electrical signals in failure-analysis tests [129], or after the fabrication as a parametric measurement, improving the investigation time because of the high repetition rate capability and the simplicity of laser experiments compared to electrical methods. The laser approach is also attractive to emulate more generally accelerated aging or radiative effects to test their robustness in hard condition environments (e.g. space, nuclear). Originally all these PLS techniques were surface techniques because of the use of laser sources in the near-infrared or visible domain for which silicon is opaque. With the emergence of femtosecond lasers at longer wavelength for which silicon is transparent, one can initiate the effects by multiphoton ionization and achieve these studies with 3D resolution. At 1.3 μm corresponding to the two-photon ionization regime, local free-carrier injection can be achieved anywhere with beams from the rear-side silicon substrate supporting the integrated circuits. Recent work have revealed that tightly focused femtosecond pulses can inject free-carrier densities exceeding 10^{19} cm^{-3} anywhere inside silicon in a self-limited sub-modification regime [130, 131, 132, 133, 134, 135]. This was exploited to develop an induced current imaging technique (so called two-photon optical beam induced current imaging) capable of characterizing integrated circuits through the polished backside of integrated circuits [136, 137, 138]. By irradiating non-volatile FLASH memory cells using pulses of only 100 nJ, the carriers generated in the cell substrate are thus attracted by the inherent vertical electric field induced by the floating gate potential and the cell could be programmed [133, 131]. For robustness studies, a benefit of laser experiments is that the total ionizing dose [139] can be easily varied with the femtosecond laser parameters (the laser energy density and number of applied pulses). Finally, ionizing radiation or aging tolerance levels for specific region of systems can be derived from test procedures. All these represent the first 3D demonstrations in the field but one can expect that similar

laser effects should be rapidly demonstrated on other silicon semiconductor devices as capacitors, SRAM, etc. We can also expect the emergence of new applications exploiting the inherent speed of the ultrafast laser-based methods. Taking electrical control anywhere locally in a micro-system (micrometer resolution), and with an extreme time precision is obviously a basis for ultrafast electronics.

Backside wafer processing. As detailed in previous section, the propagation nonlinearities of high-contrast femtosecond laser pulses in silicon prevent sufficient energy deposition to achieve modification in the bulk of the material through a plane interface [64, 36]. Obviously this holds also when damage is intended at the exit surface of the material due the bulk effects. Using 100-fs duration pulses at 1.3-μm wavelength, Lei *et al.* showed however that repeatable modifications could be produced on a gold-coating at the exit surface of a silicon wafer [140]. Despite the optical limitations, the lower damage threshold and higher absorption of the thin metal film compared to silicon made possible to demonstrate back-surface processing. A similar configuration for selective removal of gold films was also used conducted in another study at 2.09-μm wavelength [141]. By employing a single chirped volume Bragg grating for stretching and compressing the pulses, the authors investigated the pulse-duration dependence of ablation from 400 fs to 6 ns. The main conclusion was about an optimal ablation obtained with 3.2-ps pulses that can be attributed to a trade-off between the propagation nonlinearities and thermal effects observed with longer pulses. Overall these laser experiments open the perspective of through-silicon processing of CMOS-processed wafer to trim or adjust locally the functionality of the systems, a situation without any real technological alternative.

Besides these demonstrations, the enhanced absorption at the exit surface of silicon when interfaced with a metal can also lead to new solutions for additive manufacturing. This was recently shown by Chambonneau *et al.* who achieved the first semiconductor–metal laser welding with 9.8-ps pulses at 1.55-μm wavelength, demonstrated with silicon and copper [142]. The propagation of these short pulses in silicon inevitably leads to the formation of filaments. In order to characterize them, nonlinear propagation imaging in silicon was performed for various input pulse energies. This allowed the authors to determine systematically the experimental value of the nonlinear focal shift (i.e., the distance between the focus positions in the linear and nonlinear propagation regimes on the optical axis), in excellent agreement with theoretical predictions based on a modified Marburger formula [143] accounting for the nonlinear absorption losses. For all tested conditions, a precompensation of the nonlinear focal shift was proposed to optimize the energy deposition at the exit surface of silicon—corresponding to the Si-Cu interface—as shown in Figure 15. Without a precompensation of the nonlinear focal shift [dashed lines in Figure 15(b)], mediocre shear joining strength values are obtained (< 30 kPa). In stark contrast, the precompensation strategy [solid lines in Figure 15(b)] significantly increases the shear joining strength values. For the highest pulse energies tested (1 μJ), the authors reported shear joining strengths as high as 2.2 MPa, thus compatible with applications [see Figure 15(c)]. This demonstrates the importance of accounting for the nonlinear propagation in such innovative through-silicon process developments

with direct applications in microelectronics, where semiconductors and metals are the backbone materials.

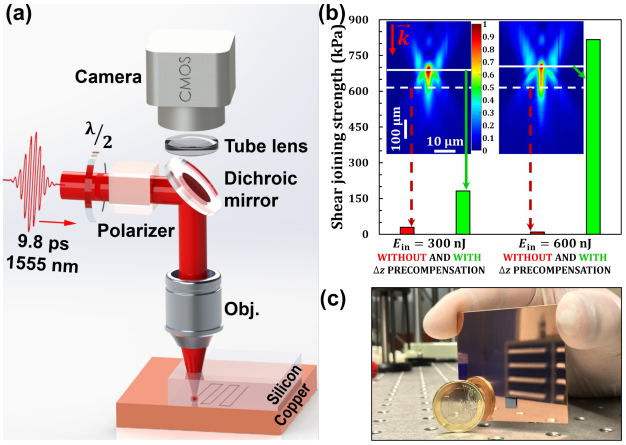

Fig. 15 Semiconductor–metal ultrafast laser welding (laser wavelength: 1.55 µm, pulse duration: 9.8 ps). (a) Schematic of the experimental arrangement. (b) Laser-induced shear joining strength between silicon and copper at different pulse energies without (in red) and with (in green) precompensation of nonlinear focal shift. The insets are the corresponding fluence distributions obtained with nonlinear propagation imaging. The solid and dashed white lines indicate the position of the Si-Cu interface in each configuration. (c) Photograph of an ultrafast-laser-welded crystalline silicon sample on copper. Reprinted with permission [142].

5.2 Toward 3D silicon photonics

3D laser writing applicable to silicon may drastically change the design and fabrication in the important field of *Silicon Photonics*. This field includes for instance silicon-on-insulator (SOI) and silicon nitride (SiNx) technologies which are rapidly progressing. However, a limitation is related to the planar lithographic methods used for fabrication. The later confine the possible architectures in two dimensions. Laser writing can provide a unique solution for new 3D designs. At short term, we can expect a flexible tool for prototyping studies which may present a real booster for the emergence of disruptive technologies and new concepts in this context.

Three-dimensional refractive index engineering and waveguide fabrication. The critical initial step for the emergence of new fabrication technologies of optical microdevices corresponds obviously to the demonstration of high-performance waveguide structures. This is the question on which process engineering efforts have concentrated recently. A first demonstration of femtosecond laser waveguide writing was provided by Pavlov *et al.* [126]. Pulses of 350-fs duration, 1.5-µm wavelength and 250-kHz repetition rate were applied with NA = 0.5. The structures were fabricated

in the longitudinal writing configuration starting from the exit surface to the entrance surface (bottom-up writing). The input and output facets of the waveguides were then prepared by polishing the surfaces. As illustrated in Figure 16, the injection of continuous light in the 20-μm diameter and 5.5-mm long structures revealed their waveguiding properties. This was consistent with an independent measurement of the refractive index changes found to be $\Delta n \approx 5 \times 10^{-4}$ for the modified channel. A comparable technique has been also implemented by Matthäus *et al.* [127]. In this study, a rough polishing process was intentionally applied on the exit surface of the sample for generating the necessary seeds for the subsequent waveguide inscription with 800-fs pulses. At an optimum pulse energy to improve the quality of waveguides, a refractive index change as large as $\Delta n = 2.5 \times 10^{-3}$ is obtained. Losses of the waveguides were estimated at 8.7 dB cm^{-1}. This is a critical performance that surely will need improvements for application developments. The light-guiding properties were additionally supported by the inscription of Y-splitters similar to those in Ref. [54]. Complementing this work, the same group has recently carried out in-depth analyses of the waveguide profiles, i.e., its refractive index profile distribution in the xy plane perpendicular to the optical axis z [128]. They also investigated the material science aspects behind the achieved silicon modification by using Raman spectroscopy [144]. Micro-spectroscopy images unambiguously exhibit the changes in the spectral ranges of 430–500 cm^{-1} and 930–1040 cm^{-1} associated with amorphous and crystalline features, respectively [145, 146]. The apparent modest decrease in crystallinity was interpreted as a disturbed crystal structure, potentially induced by defects and dislocations.

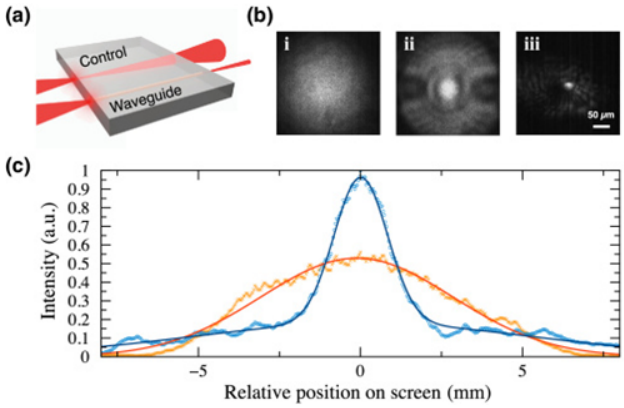

Fig. 16 Femtosecond laser waveguide writing inside silicon (laser wavelength: 1.5 μm; pulse duration: 350 fs). (a) Schematic illustration of direct coupling of continuous light at 1.5-μm wavelength into the waveguide in bulk silicon and the corresponding control experiment. (b) i, far-field image of the light after passing through silicon without waveguide. ii, far-field image of the light exiting from the end facet of the waveguide. iii, near-field image of the light exiting from the end facet of a waveguide. (c) Intensity profiles along the vertical axes of the far-field images shown in parts i, ii, and the corresponding numerical fits. Reprinted with permission from [126] ©The Optical Society.

Ultrafast optical signal switching and modulation. Laser writing of active devices will be likely an important next step for the topic. Integration of optical systems with microelectronics can provide more bandwidth for data transport and switching than any purely electronic approach. Accordingly silicon photonics and silicon-on-insulator (SOI) waveguide devices are today receiving considerable attention. In these technologies, it is the change in refractive index and absorption due to free-carrier injection by multiphoton ionization which can effectively be exploited for example for the development of ultrafast modulators and switches. Different all-optical switching methods have been demonstrated including silicon micro-ring resonators in which switching relies on the detuning of the resonance wavelength of the resonator [147, 148], photonic crystal structures for which switching is obtained by detuning the optical band gap through carrier injection [149], or by photo-induced carrier injection in one of the arm of interferometric systems [150]. In principle, all these approaches can be translated in 3D systems fabricated by laser writing (see above). However, to really extend signal control and processing at the time scale of the pulse duration, one requires a reversing of the induced effects approximately as fast as they can be induced. In practice, free-carrier lifetime limits the switching or modulation speed of devices based on free-carrier injection. The latter depends strongly on the materials and geometry of the nano/microstructures. We have seen in section 3.2 that reported values for carrier lifetime in silicon are typically on the order of nanoseconds for excited volumes of micrometer dimensions [81] but solutions are envisioned to solve this limitation. Ultimately, light-field-induced electron tunneling can be a potential carrier injection mechanism with switching on and off at the time scale of the optical cycle. Looking to the future, this may represent a new route for microelectronics and up to petahertz-bandwidth information processing. Recent high profile fundamental experiments based on attosecond metrology on dielectrics [151, 152] and silicon [153] pave the way in this new horizon of applications.

6 Summary and outlook

A major conclusion is the incapacity to achieve ultrafast laser modifications in semiconductors similar to those observed in dielectrics with tightly focused highly-contrasted infrared pulses. We have reviewed the factors and propagation nonlinearities which lower the apparent intensity inside high refractive index narrow-gap semiconductors. We have also briefly described the results of multiple groups that moved to unconventional configurations (including solid-immersion focusing), longer pulses (from picosecond to nanosecond regimes) or ultrashort pulse sequences to demonstrate increased energy deposition and achieve internal modifications in silicon.

It is worth noting that the first attempts of 3D machining with infrared femtosecond pulses were performed a decade ago (for tentative waveguide writing in bulk Si) [34]. However, the door finally opens only recently to the ultrafast regime. It is also interesting to note that the first ever ultrafast modifications deep inside c-Si exhibit

a negative index change [36] (exceeding few percents) and some works demonstrated that modifications can take the form of periodic nanostructures [121, 122]. These features are very similar to the results reported with nanograting formation in dielectrics [16, 15] and discussed in chapter 5.

This definitely tends to show that technologies as the direct writing of photonics micro-devices similar to those developed for dielectrics could be translated in semiconductors provided that practical solutions are found to enhance of the delivered intensity (and/or energy densities) of long-wavelength femtosecond pulses inside semiconductors. This remains the most important challenge to meet for the future of *Silicon Photonics*.

For more general perspectives of this work, the plasma characteristics achieved with ultrafast light hold already great promises for studies in microelectronics, ultrafast signal processing and silicon photonics as described in section 5. When regimes above breakdown will be routinely accessed in semiconductors, we envision that laser writing can become a new booster for innovative developments in the semiconductor sector where microfabrication is largely dominated by lithography methods. The integration of photonic, fluidic and electronic functionalities by 3D femtosecond laser writing in Si must open the way to hybrid monolithic devices. A potential is already identified to facilitate prototyping studies of emerging new concepts for co-designed electronics and microfluidics seen as solution for critical thermal management in most advanced chip technologies [154, 155].

References

1. K. M. Davis, K. Miura, N. Sugimoto, and K. Hirao. Writing waveguides in glass with a femtosecond laser. *Opt. Lett.*, 21:1729, 1996.
2. K. Miura, J. Qiu, H. Inouye, T. Mitsuyu, and K. Hirao. Photowritten optical waveguides in various glasses with ultrashort pulse laser. *Appl. Phys. Lett.*, 71(23):3329, 1997.
3. L. Sudrie, A. Couairon, M. Franco, B. Lamouroux, B. Prade, S. Tzortzakis, and A. Mysyrowicz. Femtosecond laser-induced damage and filamentary propagation in fused silica. *Phys. Rev. Lett.*, 89(18):186601, 2002.
4. R. R. Gattass and E. Mazur. Femtosecond laser micromachining in transparent materials. *Nat. Photonics*, 2:219–225, 2008.
5. K. Sugioka and Y. Cheng. Femtosecond laser three-dimensional micro- and nanofabrication. *Appl. Phys. Rev.*, 1:041303, 2014.
6. M. Beresna, M. Gecevičius, and P. G. Kazansky. Ultrafast laser direct writing and nanostructuring in transparent materials. *Adv. Opt. Phot.*, 6(3):293–339, 2014.
7. K. Sugioka and Y. Cheng. Ultrafast lasers : reliable tools for advanced materials processing. *Light: Science & Applications*, 3:e149, 2014.
8. B. Poumellec, M. Lancry, A. Chahid-Erraji, and P. G Kazansky. Modification thresholds in femtosecond laser processing of pure silica: review of dependencies on laser parameters. *Opt. Mat. Express*, 1(4):766–782, 2011.
9. S. M. Eaton, G. Cerullo, and R. Osellame. Fundamentals of femtosecond laser modification of bulk dielectrics. *Femtosecond Laser Micromachining*, pages 3–18, 2012.
10. J. W. Chan, T. Huser, S. Risbud, and D. M. Krol. Structural changes in fused silica after exposure to focused femtosecond laser pulses. *Opt. Lett.*, 26(21):1726–1728, 2001.
11. F. Chen and J. R. Vazquez de Aldana. Optical waveguides in crystalline dielectric materials produced by femtosecond-laser micromachining. *Laser Photonics Rev.*, 8(2):251–275, 2014.

12. T. Meany, M. Gräfe, R. Heilmann, A. Perez-Leija, S. Gross, M. J. Steel, M. J. Withford, and A. Szameit. Laser written circuits for quantum photonics. *Laser Photonics Rev.*, 9(4):363–384, 2015.
13. D. Grojo, M. Gertsvolf, S. Lei, T. Barillot, D. M. Rayner, and P. B. Corkum. Exciton-seeded multiphoton ionization in bulk SiO_2. *Phys. Rev. B*, 81(21):212301, 2010.
14. Roberto Osellame, Giulio Cerullo, and Roberta Ramponi. *Femtosecond laser micromachining: photonic and microfluidic devices in transparent materials*. Springer, Berlin, Heidelberg, 2012.
15. Y. Shimotsuma, P. G. Kazansky, J. Qiu, and K. Hirao. Self-organized nanogratings in glass irradiated by ultrashort light pulses. *Phys. Rev. Lett.*, 91(24):247405, 2003.
16. V. Bhardwaj, E. Simova, P. Rajeev, C. Hnatovsky, R. Taylor, D. Rayner, and P. Corkum. Optically Produced Arrays of Planar Nanostructures inside Fused Silica. *Phys. Rev. Lett.*, 96(5):057404, 2006.
17. E. Bricchi, B. G. Klappauf, and P. G. Kazansky. Form birefringence and negative index change created by femtosecond direct writing in transparent materials. *Opt. Lett.*, 29(1):119, 2004.
18. D. Grojo, M. Gertsvolf, H. Jean-Ruel, S. Lei, L. Ramunno, D. M. Rayner, and P. B. Corkum. Self-controlled formation of microlenses by optical breakdown inside wide-band-gap materials. *Appl. Phys. Lett.*, 93(24):243118, 2008.
19. T. Barillot, D. Grojo, M. Gertsvolf, S. Lei, D. M Rayner, and P. B. Corkum. High refractive index modification of SiO2 created by femtosecond laser nanostructuring. *J.Phys. B*, 43(12):125401, 2010.
20. J. Zhang, M. Gecevičius, M. Beresna, and P. G. Kazansky. Seemingly Unlimited Lifetime Data Storage in Nanostructured Glass. *Phys. Rev. Lett.*, 112(3):033901, 2014.
21. G. Corrielli, A. Crespi, R. Geremia, R. Ramponi, L. Sansoni, A. Santinelli, P. Mataloni, F. Sciarrino, and R. Osellame. Rotated waveplates in integrated waveguide optics. *Nat. Commun.*, 5:4249, 2014.
22. Saulius Juodkazis, Vygantas Mizeikis, and Hiroaki Misawa. Three-dimensional microfabrication of materials by femtosecond lasers for photonics applications. *J. Appl. Phys.*, 106(5):8, 2009.
23. S. Juodkazis, K. Nishimura, S. Tanaka, H. Misawa, E. G. Gamaly, B. Luther-Davies, L. Hallo, P. Nicolai, and V. T. Tikhonchuk. Laser-induced microexplosion confined in the bulk of a sapphire cystal: Evidence of multimegabar pressures. *Phys. Rev. Lett.*, 96(16), 2006.
24. E. G. Gamaly, B. Luther-Davies, L. Hallo, P. Nicolai, and V. T. Tikhonchuk. Laser-matter interaction in the bulk of a transparent solid: Confined microexplosion and void formation. *Phys. Rev. B*, 73(21):214101, 2006.
25. C. Hnatovsky, E. Simova, P. P. Rajeev, D. M. Rayner, P. B. Corkum, and R. S. Taylor. Femtosecond laser writing of porous capillaries inside fused silica glass. *Opt. Lett.*, 32(11):1459–61, 2007.
26. M. K. Bhuyan, F. Courvoisier, P. A. Lacourt, M. Jacquot, R. Salut, L. Furfaro, and J. M. Dudley. High aspect ratio nanochannel machining using single shot femtosecond Bessel beams. *Appl. Phys. Lett.*, 97(8):4–7, 2010.
27. B.-B. Xu, Y.-L. Zhang, H. Xia, W.-F. Dong, H. Ding, and H.-B. Sun. Fabrication and multifunction integration of microfluidic chips by femtosecond laser direct writing. *Lab. Chip*, 13(9):1677, 2013.
28. A. Vailionis, E. G Gamaly, V. Mizeikis, W. Yang, A. V Rode, and S. Juodkazis. Evidence of superdense aluminium synthesized by ultrafast microexplosion. *Nat. Commun.*, 2:445, 2011.
29. M. Chambonneau, D. Grojo, O. Tokel, F. O. Ilday, S. Tzortzakis, and S. Nolte. In-Volume Laser Direct Writing of Silicon—Challenges and Opportunities. *Laser Photonics Rev.*, 15:2100140, 2021.
30. D. Grojo, S. Leyder, P. Delaporte, W. Marine, M. Sentis, and O. Utéza. Long-wavelength multiphoton ionization inside band-gap solids. *Phys. Rev. B*, 88(19):195135, 2013.
31. A. Wang, A. Das, and D. Grojo. Temporal-contrast imperfections as drivers for ultrafast laser modifications in bulk silicon. *Phys. Rev. Res.*, 033023, 2020.

32. A. Das, A. Wang, O. Uteza, and D. Grojo. Pulse-duration dependence of laser-induced modifications inside silicon. *Opt. Express*, 28(18):26623, 2020.
33. O. Tokel, A. Turnali, G. Makey, P. Elahi, T. Çolakoğlu, E. Ergeçen, Ö. Yavuz, R. Hübner, M. Z. Borra, I. Pavlov, A. Bek, R. Turan, D. K. Kesim, S. Tozburun, S. Ilday, and F. O. Ilday. In-chip microstructures and photonic devices fabricated by nonlinear laser lithography deep inside silicon. *Nat. Photon.*, 11(10):639–645, 2017.
34. A. H. Nejadmalayeri, P. R. Herman, J. Burghoff, M. Will, S. Nolte, and A. Tünnermann. Inscription of optical waveguides in crystalline silicon by mid-infrared femtosecond laser pulses. *Opt. Lett.*, 30(9):964, 2005.
35. VV Parsi Sreenivas, M Bülters, and RB Bergmann. Microsized subsurface modification of mono-crystalline silicon via non-linear absorption. *J. Eur. Opt. Soc.*, 7(12035), 2012.
36. M. Chanal, V. Yu Fedorov, M. Chambonneau, R. Clady, S. Tzortzakis, and D. Grojo. Crossing the threshold of ultrafast laser writing in bulk silicon. *Nat. Commun.*, 8:773, 2017.
37. E. Ohmura, F. Fukuyo, K. Fukumitsu, and H. Morita. Internal modified-layer formation mechanism into silicon with nanosecond laser. *J. Achiev. Mat. Manuf. Eng.*, 17(1):381–384, 2006.
38. D. Lide, editor. *Handbook of chemistry and physics, 85th ed.* CRC Press, Boca, Raton (FL), USA, 2003.
39. Y. P. Varshni. Temperature dependence of the energy gap in semiconductors. *Physica*, 34(1):149–154, 1967.
40. P. C. Verburg, G. R. B. E. Romer, and A. J. Huis in 'T Veld. Two-temperature model for pulsed-laser-induced subsurface modifications in Si. *Appl. Phys. A*, 114(4):1135–1143, 2014.
41. P. C. Verburg, G. R. B. E. Römer, and A. J. Huis in 't Veld. Two-photon-induced internal modification of silicon by erbium-doped fiber laser. *Opt. Express*, 22(18):21958, 2014.
42. P. C. Verburg, L. A. Smillie, G. R. B. E. Römer, B. Haberl, J. E. Bradby, J. S. Williams, and A. J. Huis in 't Veld. Crystal structure of laser-induced subsurface modifications in Si. *Appl. Phys. A*, 120(2):683–691, 2015.
43. Q. Li, M. Chambonneau, M. Chanal, and D. Grojo. Quantitative-phase microscopy of nanosecond laser-induced micro-modifications inside silicon. *Appl. Opt.*, 55(33):9577, 2016.
44. H. Kiyota, K. Hara, M. Jankowski, and M. M. Fejer. Numerical simulation and validation of subsurface modification and crack formation induced by nanosecond-pulsed laser processing in monocrystalline silicon. *J. Appl. Phys.*, 127(8):085106, 2020.
45. H. Iwata, D. Kawaguchi, and H. Saka. Electron microscopy of voids in Si formed by permeable pulse laser irradiation. *Microscopy*, 66(5):328–336, 2017.
46. H. Iwata, D. Kawaguchi, and H. Saka. Crystal structures of high-pressure phases formed in Si by laser irradiation. *Microscopy*, 67(1):30–36, 2018.
47. Ahmet Turnali, Mertcan Han, and Onur Tokel. Laser-written depressed-cladding waveguides deep inside bulk silicon. *J. Opt. Soc. Am. B*, 36(4):966, 2019.
48. M. Chambonneau, Q. Li, M. Chanal, N. Sanner, and D. Grojo. Writing waveguides inside monolithic crystalline silicon with nanosecond laser pulses. *Opt. Lett.*, 41(21):4875, 2016.
49. Y. Fujii, F. Fukuyo, K. Fukumitsu, and N. Uchiyama. Method for dicing a substrate, 2012. US Patent 8,268,704 B2.
50. Y. Izawa, S. Tanaka, H. Kikuchi, Y. Tsurumi, N. Miyanaga, M. Esashi, and M. Fujita. Debris-free in-air laser dicing for multi-layer MEMS by perforated internal transformation and thermally-induced crack propagation. In *MEMS 2008. IEEE 21st International Conference on Micro Electro Mechanical Systems*, pages 822–827. IEEE, 2008.
51. M. Finarov, E. Tirosh, G. Dishon, and A. Gusarov. A method and apparatus for internal marking of ingots and wafers, 2015. Patent WO 125134 A1.
52. O. Tokel, A. Turnali, I. Pavlov, S. Tozburun, I. Akca, and F.O. Ilday. Laser-Writing in Silicon for 3D Information Processing. *Arxiv*, 1409.2827v, 2014.
53. M. Chambonneau, D. Richter, S. Nolte, and D. Grojo. Inscribing diffraction gratings in bulk silicon with nanosecond laser pulses. *Opt. Lett.*, 43(24):6069, 2018.
54. D. Grojo and M. Chambonneau. Methods and systems for optical functionalisation of a sample made of semiconductor material, 2019. US Patent 10,509,168.

55. X. Wang, X. Yu, H. Shi, X. Tian, M. Chambonneau, D Grojo, B. DePaola, M. Berg, and S. Lei. Characterization and control of laser induced modification inside silicon. *J. Las. Appl.*, 31(2):022601, 2019.
56. X. Wang, X. Yu, M. J. Berg, P. Chen, B. Lacroix, S. Fathpour, and S. Lei. Curved waveguides in silicon written by a shaped laser beam. *Opt. Express*, 29(10):14201, 2021.
57. M. Chambonneau, X. Wang, X. Yu, Q. Li, D. Chaudanson, S. Lei, and D. Grojo. Positive- and negative-tone structuring of crystalline silicon by laser-assisted chemical etching. *Opt. Lett.*, 44(7):1619, 2019.
58. B. Dang, M. S. Bakir, D. C. Sekar, C. R. King, Jr, and J. D. Meindl. Integrated Microfluidic Cooling and Interconnects for 2D and 3D Chips. *IEEE Tr. Adv. Pack.*, 33(1):79–87, 2010.
59. M Lipson. Guiding, modulating, and emitting light on Silicon-challenges and opportunities. *J. Lightwave Tech.*, 23(12):4222–4238, 2005.
60. M. A. Foster, A. C. Turner, J. E. Sharping, B. S. Schmidt, M. Lipson, and A. L. Gaeta. Broad-band optical parametric gain on a silicon photonic chip. *Nature*, 441(7096):960–963, 2006.
61. M. A. Foster, R. Salem, D. F. Geraghty, A. C. Turner-Foster, M. Lipson, and A. L. Gaeta. Silicon-chip-based ultrafast optical oscilloscope. *Nature*, 456(7218):81–84, 2008.
62. M. Kolesik and J. V. Moloney. Nonlinear optical pulse propagation simulation: From Maxwell's to unidirectional equations. *Phys. Rev. E*, 70:036604, 2004.
63. J Del Hoyo, a Ruiz de la Cruz, E Grace, a Ferrer, J Siegel, a Pasquazi, G Assanto, and J Solis. Rapid assessment of nonlinear optical propagation effects in dielectrics. *Sci. Rep.*, 5:7650, 2015.
64. V. Yu. Fedorov, M. Chanal, D. Grojo, and S. Tzortzakis. Accessing Extreme Spatiotemporal Localization of High-Power Laser Radiation through Transformation Optics and Scalar Wave Equations. *Phys. Rev. Lett.*, 117(4):043902, 2016.
65. E. V. Zavedeev, V. V. Kononenko, and V. I. Konov. Delocalization of femtosecond laser radiation in crystalline Si in the mid-IR range. *Laser Phys.*, 26(1):016101, 2016.
66. V. V Kononenko, V. V Konov, and E. M Dianov. Delocalization of femtosecond radiation in silicon. *Opt. Lett.*, 37(16):3369–71, 2012.
67. A. Mouskeftaras, A. V. Rode, R. Clady, M. Sentis, O. Utéza, and D. Grojo. Self-limited underdense microplasmas in bulk silicon induced by ultrashort laser pulses. *Appl. Phys. Lett.*, 105:191103, 2014.
68. A. D. Bristow, N. Rotenberg, and H. M. van Driel. Two-photon absorption and Kerr coefficients of silicon for 850 - 2200 nm. *Appl. Phys. Lett.*, 90(19):191104, 2007.
69. D. Milam. Review and assessment of measured values of the nonlinear refractive-index coefficient of fused silica. *Appl. Opt.*, 37(3):546–550, 1998.
70. A. Dragomir, J. G. McInerney, D. N. Nikogosyan, and P. G. Kazansky. Two-photon absorption properties of commercial fused silica and germanosilicate glass at 264 nm. *Appl. Phys. Lett.*, 80(7):1114–1116, 2002.
71. X. Gai, Y. Yu, B. Kuyken, P. Ma, S. J. Madden, J. Van Campenhout, P. Verheyen, G. Roelkens, R. Baets, and B. Luther-Davies. Nonlinear absorption and refraction in crystalline silicon in the mid-infrared. *Laser Photonics Rev.*, 7(6):1054–1064, 2013.
72. S. Pearl, N. Rotenberg, and H. M. Van Driel. Three photon absorption in silicon for 2300-3300 nm. *Appl. Phys. Lett.*, 93(13):131102, 2008.
73. J. Jasapara, A. Nampoothiri, W. Rudolph, D. Ristau, and K. Starke. Femtosecond laser pulse induced breakdown in dielectric thin films. *Phys. Rev. B*, 63(4):1–5, 2001.
74. S. Mitra, M. Chanal, R. Clady, A. Mouskeftaras, and D. Grojo. Millijoule femtosecond micro-Bessel beams for ultra-high aspect ratio machining. *Appl. Optics*, 54(24):7358, 2015.
75. X. Mao, S. S. Mao, and R. E. Russo. Imaging femtosecond laser-induced electronic excitation in glass. *Appl. Phys. Lett.*, 82(5):697–699, 2003.
76. Q. Sun, H. Jiang, Y. Liu, Z. Wu, H. Yang, and Q. Gong. Measurement of the collision time of dense electronic plasma induced by a femtosecond laser in fused silica. *Opt. Lett.*, 30(3):320–2, 2005.

77. W. Gawelda, D. Puerto, J. Siegel, A. Ferrer, A. Ruiz de la Cruz, H. Fernandez, and J. Solis. Ultrafast imaging of transient electronic plasmas produced in conditions of femtosecond waveguide writing in dielectrics. *Appl. Phys. Lett.*, 93(12):2008–2010, 2008.
78. P. Martin, S. Guizard, Ph. Daguzan, G. Petite, P. D'Oliveira, P. Meynadier, and M. Perdrix. Subpicosecond study of carrier trapping dynamics in wide-band-gap crystals. *Phys. Rev. B*, 55(9):5799–5810, 1997.
79. P. Audebert, Ph Daguzan, A. Dos Santos, J. C. Gauthier, J. P. Geindre, S. Guizard, G. Hamoniaux, K. Krastev, P. Martin, G. Petite, and A. Antonetti. Space-time observation of an electron gas in SiO2. *Phys. Rev. Lett.*, 73(14):1990–1993, 1994.
80. D. G. Papazoglou and S. Tzortzakis. In-line holography for the characterization of ultrafast laser filamentation in transparent media. *Appl. Phys. Lett.*, 93(4):2–5, 2008.
81. A. Mouskeftaras, M. Chanal, M. Chambonneau, R. Clady, and O. Utéza. Direct measurement of ambipolar diffusion in bulk silicon by ultrafast infrared imaging of laser-induced microplasmas. *Appl. Phys. Lett.*, 108:041107, 2016.
82. M. J. Kerr and A. Cuevas. General parameterization of Auger recombination in crystalline silicon. *J. Appl. Phys.*, 91(3):2473–2480, 2002.
83. A. Wang, A. Das, J. Hermann, and D. Grojo. Three-dimensional luminescence microscopy for quantitative plasma characterization in bulk semiconductors. *Appl. Phys. Lett.*, 119(4):041108, 2021.
84. W. Van Roosbroeck and W. Shockley. Photon-radiative recombination of electrons and holes in germanium. *Phys. Rev.*, 94(6):1558, 1954.
85. D. Abdollahpour, D. G. Papazoglou, and S. Tzortzakis. Four-dimensional visualization of single and multiple laser filaments using in-line holographic microscopy. *Phys. Rev. A*, 84(5):053809, 2011.
86. T. Balciunas, A. Melninkaitis, G. Tamosauskas, and V. Sirutkaitis. Time-resolved off-axis digital holography for characterization of ultrafast phenomena in water. *Opt. Lett.*, 33(1):58, 2008.
87. O. Tokel, A. Turnali, P. Deminskyi, S. Ilday, and F. O. Ilday. Laser writing of nanostructures deep inside gallium arsenide. In *Conference on Lasers and Electro-Optics/Pacific Rim*, pages W1E–2. Optical Society of America, 2018.
88. S. Leyder, D. Grojo, P. Delaporte, W. Marine, M. Sentis, and O. Utéza. Non-linear absorption of focused femtosecond laser pulses at 1.3μm inside silicon Independence on doping concentration. *Appl. Surf. Sci.*, 278:13–18, 2013.
89. D. Faccio, M. Clerici, A. Averchi, O. Jedrkiewicz, S. Tzortzakis, D. G. Papazoglou, F. Bragheri, L. Tartara, A. Trita, S. Henin, I. Cristiani, A. Couairon, and P. Di Trapani. Kerr-induced spontaneous Bessel beam formation in the regime of strong two-photon absorption. *Opt. Express*, 16(11):8213–8, 2008.
90. V. V. Kononenko, E. V. Zavedeev, and V. M. Gololobov. The effect of light-induced plasma on propagation of intense fs laser radiation in c-Si. *Appl. Phys. A*, 122:293, 2016.
91. D. Grojo, N. Sandeau, L. Boarino, C. Constantinescu, N. De Leo, M. Laus, and K. Sparnacci. Bessel-like photonic nanojets from core-shell sub-wavelength spheres. *Opt. Lett.*, 39(13):3989, 2014.
92. D. Austin, K. Kafka, C. I. Blaga, L. F. Dimauro, and E. Chowdhury. Measurement of femtosecond laser damage thresholds at mid IR wavelengths. In *Proc. SPIE*, volume 9237, page 92370V, 2014.
93. M. Garcia-Lechuga, N. Casquero, A. Wang, D. Grojo, and J. Siegel. Deep Silicon Amorphization Induced by Femtosecond Laser Pulses up to the Mid-Infrared. *Adv. Opt. Mat.*, 2100400, 2021.
94. R. M. Herman and T. A. Wiggins. Production and uses of diffractionless beams. *J. Opt. Soc. Am. A*, 8(6):932, 1991.
95. A. Marcinkevičiūtė, V. Jukna, R. Šuminas, N. Garejev, G. Tamošauskas, and A. Dubietis. Femtosecond filamentation and supercontinuum generation in bulk silicon. *Opt. Lett.*, 44(6):1343, 2019.

96. V. Kadan, S. Pavlova, I. Pavlov, H. Rezaei, Ö. Ilday, and I. Blonskyi. Spatio-temporal dynamics of femtosecond laser pulses at 1550 nm wavelength in crystal silicon. *Appl. Phys. A*, 124(8):560, 2018.
97. M. Garcia-Lechuga, O. Utéza, N. Sanner, and D. Grojo. Evidencing the nonlinearity independence of resolution in femtosecond laser ablation. *Opt. Lett.*, 45(4):952, 2020.
98. Mario Garcia-Lechuga and David Grojo. Simple and robust method for determination of laser fluence thresholds for material modifications: an extension of liu's approach to imperfect beams. *Open Research Europe*, 1:7, 2021.
99. R. A. Richter, N. Tolstik, S. Rigaud, P. D. Valle, A. Erbe, P. Ebbinghaus, I. Astrauskas, V. Kalashnikov, E. Sorokin, and I. T. Sorokina. Sub-surface modifications in silicon with ultra-short pulsed lasers above 2 µm. *J. Opt. Soc. Am. B*, 37(9):2543, 2020.
100. R Dekker, N Usechak, M Först, and A Driessen. Ultrafast nonlinear all-optical processes in silicon-on-insulator waveguides. *J. Phys. D*, 40(14):R249–R271, 2007.
101. F. Gholami, S. Zlatanovic, A. Simic, L. Liu, D. Borlaug, N. Alic, M. P. Nezhad, Y. Fainman, and S. Radic. Third-order nonlinearity in silicon beyond 2350 nm. *Appl. Phys. Lett.*, 99(8):081102, 2011.
102. Q. Lin, J. Zhang, G. Piredda, R. W. Boyd, P. M. Fauchet, and G. P. Agrawal. Dispersion of silicon nonlinearities in the near infrared region. *Appl. Phys. Lett.*, 91(2):021111, 2007.
103. T. Wang, N. Venkatram, J. Gosciniak, Y. Cui, G. Qian, W. Ji, and D. T. H. Tan. Multi-photon absorption and third-order nonlinearity in silicon at mid-infrared wavelengths. *Opt. Express*, 21(26):32192–8, 2013.
104. Q. Li, M. Chambonneau, M. Blothe, H. Gross, and S. Nolte. Flexible, fast, and benchmarked vectorial model for focused laser beams. *Appl. Opt.*, 60(13):3954, 2021.
105. M. Chambonneau, M. Blothe, Q. Li, V. Yu. Fedorov, T. Heuermann, M. Gebhardt, C. Gaida, S. Tertelmann, F. Sotier, J. Limpert, S. Tzortzakis, and S. Nolte. Transverse ultrafast laser inscription in bulk silicon. *Phys. Rev. Res.*, 3:043037, 2021.
106. D. Faccio, E. Rubino, A. Lotti, A. Couairon, A. Dubietis, G. Tamošauskas, D. G. Papazoglou, and S. Tzortzakis. Nonlinear light-matter interaction with femtosecond high-angle Bessel beams. *Phys. Rev. A*, 85(3):033829, 2012.
107. D. Grojo, A. Mouskeftaras, P. Delaporte, and S. Lei. Limitations to laser machining of silicon using femtosecond micro-Bessel beams in the infrared. *J. Appl. Phys.*, 117(15):153105, 2015.
108. M. K. Bhuyan, P. K. Velpula, J. P. Colombier, T. Olivier, N. Faure, and R. Stoian. Single-shot high aspect ratio bulk nanostructuring of fused silica using chirp-controlled ultrafast laser Bessel beams. *Appl. Phys. Lett.*, 104:021107, 2014.
109. J. Amako, D. Sawaki, and E. Fujii. Microstructuring transparent materials by use of non-diffracting ultrashort pulse beams generated by diffractive optics. *J. Opt. Soc. Am. B*, 20(12):2562, 2003.
110. M. Duocastella and C.B. Arnold. Bessel and annular beams for materials processing. *Laser Photonics Rev.*, 6(5):607–621, 2012.
111. Fei He, Junjie Yu, Yuanxin Tan, Wei Chu, Changhe Zhou, Ya Cheng, and Koji Sugioka. Tailoring femtosecond 1.5-μm Bessel beams for manufacturing high-aspect-ratio through-silicon vias. *Sci. Rep.*, 7(1):40785, 2017.
112. J. Bonse, S. Baudach, J. Krüger, W. Kautek, and M. Lenzner. Femtosecond laser ablation of silicon–modification thresholds and morphology. *Appl. Phys. A*, 74(1):19–25, 2002.
113. M. Dinu, F. Quochi, and H. Garcia. Third-order nonlinearities in silicon at telecom wavelengths. *Appl. Phys. Lett.*, 82(18):2954, 2003.
114. D. G. Papazoglou, N. K Efremidis, D. N Christodoulides, and S. Tzortzakis. Observation of abruptly autofocusing waves. *Opt. Lett.*, 36(10):1842–1844, 2011.
115. P. Panagiotopoulos, A. Couairon, M. Kolesik, D. G. Papazoglou, J. V. Moloney, and S. Tzortzakis. Nonlinear plasma-assisted collapse of ring-Airy wave packets. *Phys. Rev. A*, 93:033808, 2016.
116. K. A. Serrels, E. Ramsay, R. J. Warburton, and D. T. Reid. Nanoscale optical microscopy in the vectorial focusing regime. *Nat. Photonics*, 2(5):311–314, 2008.

117. Krishna Agarwal, Rui Chen, Lian Ser Koh, Colin J.R. Sheppard, and Xudong Chen. Crossing the Resolution Limit in Near-Infrared Imaging of Silicon Chips: Targeting 10-nm Node Technology. *Phys. Rev. X*, 5(2):021014, 2015.
118. N. Bloembergen. Role of Cracks, Pores, and Absorbing Inclusions on Laser Induced Damage Threshold at Surfaces of Transparent Dielectrics. *Appl. Opt.*, 12(4):661, 1973.
119. H. Kämmer, G. Matthäus, S. Nolte, M. Chanal, O. Utéza, and D. Grojo. In-volume structuring of silicon using picosecond laser pulses. *Appl. Phys. A*, 124(4):302, 2018.
120. E.V. Zavedeev, V.V. Kononenko, and V.I. Konov. Delocalization of femtosecond laser radiation in crystalline si in the mid-ir range. *Las. Phys.*, 26(1):016101, 2015.
121. M. Mori, Y. Shimotsuma, T. Sei, M. Sakakura, K. Miura, and H. Udono. Tailoring thermoelectric properties of nanostructured crystal silicon fabricated by infrared femtosecond laser direct writing. *Phys. Status Solidi A*, 212(4):715–721, 2015.
122. Y. Shimotsuma, T. Sei, M. Mori, M. Sakakura, and K. Miura. Self-organization of polarization-dependent periodic nanostructures embedded in III–V semiconductor materials. *Appl. Phys. A*, 122(3):159, 2016.
123. K. Sugioka, M. Iida, H. Takai, and K. Micorikawa. Efficient microwelding of glass substrates by ultrafast laser irradiation using a double-pulse train. *Opt. Lett.*, 36(14):2734, 2011.
124. J. Peng, D. Grojo, D. M. Rayner, and P. B. Corkum. Control of energy deposition in femtosecond laser dielectric interactions. *Appl. Phys. Lett.*, 102(16):161105, 2013.
125. A. Wang, A. Das, and D. Grojo. Ultrafast laser writing deep inside silicon with thz-repetition-rate trains of pulses. *Research*, 2020, 2020.
126. I. Pavlov, O. Tokel, S. Pavlova, V. Kadan, G. Makey, A. Turnali, Ö. Yavuz, and F. Ö. Ilday. Femtosecond laser written waveguides deep inside silicon. *Opt. Lett.*, 42(15):3028, 2017.
127. G. Matthäus, H. Kämmer, K. A. Lammers, C. Vetter, W. Watanabe, and S. Nolte. Inscription of silicon waveguides using picosecond pulses. *Opt. Express*, 26(18):24089, 2018.
128. A. Alberucci, N. Alasgarzade, M. Chambonneau, M. Blothe, H. Kämmer, G. Matthäus, C. P. Jisha, and S. Nolte. In-Depth Optical Characterization of Femtosecond-Written Waveguides in Silicon. *Phys. Rev. Appl.*, 14(2):024078, 2020.
129. P. Perdu, R. Desplats, K. Sanchez, F. Beaudoin, D. Lewis, V. Pouget, A. Douin, and P. Fouillat. Identification of some key parameters for photoelectric laser stimulation of ic: an experimental approach. In *Proceedings of the 12th International Symposium on the Physical and Failure Analysis of Integrated Circuits, 2005.*, pages 21–26. IEEE, 2005.
130. D. McMorrow, W. T. Lotshaw, J. S. Melinger, S. Buchner, and R. L. Pease. Subbandgap laser-induced single event effects: Carrier generation via two-photon absorption. *IEEE Transactions on Nuclear Science*, 49 I(6):3002–3008, 2002.
131. M. Chambonneau, S. Souiki-Figuigui, P. Chiquet, V. Della Marca, J. Postel-Pellerin, P. Canet, J.-M. Portal, and D. Grojo. Suppressing the memory state of floating gate transistors with repeated femtosecond laser backside irradiations. *Appl. Phys. Lett.*, 110(16):6, 2017.
132. P. Chiquet, M. Chambonneau, V. Della Marca, J. Postel-Pellerin, P. Canet, S. Souiki-Figuigui, G. Idda, J. M. Portal, and D. Grojo. Phenomenological modelling of non-volatile memory threshold voltage shift induced by nonlinear ionization with a femtosecond laser. *Sci. Rep.*, 9(1):1–10, 2019.
133. V. Della Marca, M Chambonneau, S. Souiki-Figuigui, J. Postel-Pellerin, P Canet, P Chiquet, E Kussener, F. Yengui, R. Wacquez, D. Grojo, J.-M. Portal, and M. Lisart. NVM cell degradation induced by femtosecond laser backside irradiation for reliability tests. In *2016 IEEE International Reliability Physics Symposium (IRPS)*, volume 2016-Septe, pages 7B–4–1–7B–4–7. IEEE, 2016.
134. J. M. Hales, J. D. Cressler, D. McMorrow, A. Khachatrian, S. Buchner, J. Warner, A. Ildefonso, G. N. Tzintzarov, D. Nergui, D. M. Monahan, and S. D. LaLumondiere. New Approach for Pulsed-Laser Testing That Mimics Heavy-Ion Charge Deposition Profiles. *IEEE Transactions on Nuclear Science*, 67(1):81–90, 2020.
135. L. D. Ryder, K. L. Ryder, A. L. Sternberg, J. A. Kozub, H. Gong, E. X. Zhang, D. Linten, J. Mitard, R. A. Weller, R. D. Schrimpf, S. M. Weiss, and R. A. Reed. Polarization Dependence of Pulsed Laser-Induced SEEs in SOI FinFETs. *IEEE Transactions on Nuclear Science*, 67(1):38–43, 2020.

136. C Xu and W Denk. Two-photon optical beam induced current imaging through the backside of integrated circuits. *Appl. Phys. Lett.*, 71(18):2578–2580, 1997.
137. P. Parkinson, Y. H. Lee, L. Fu, S. Breuer, H. H. Tan, and C. Jagadish. Three-dimensional in situ photocurrent mapping for nanowire photovoltaics. *Nano Lett.*, 13(4):1405–1409, 2013.
138. E Ramsay, N Pleynet, D Xiao, R J Warburton, and D T Reid. Two-photon optical-beam-induced current solid-immersion imaging of a silicon flip chip with a resolution of 325 nm. *Opt. Lett.*, 30(1):26–28, 2005.
139. E Simoen, Marc Gaillardin, Philippe Paillet, Robert a Reed, Ronald D Schrimpf, Michael L Alles, Farah El-Mamouni, Daniel M Fleetwood, a Griffoni, and C Claeys. Radiation Effects in Advanced Multiple Gate and Silicon-on-Insulator Transistors. *IEEE Transactions on Nuclear Science*, 60(3):1970–1991, 2013.
140. S. Lei, D. Grojo, J. Ma, X. Yu, and H. Wu. Femtosecond Laser Backside Ablation of Gold Film on Silicon Substrate. *Procedia Manufacturing*, 5:594–608, 2016.
141. I. Astrauskas, B. Považay, A. Baltuška, and A. Pugžlys. Influence of 2.09-μm pulse duration on through-silicon laser ablation of thin metal coatings. *Opt. Las. Tech.*, 133:106535, 2021.
142. M. Chambonneau, Q. Li, V. Yu Fedorov, M. Blothe, K. Schaarschmidt, M. Lorenz, S. Tzortzakis, and S. Nolte. Taming Ultrafast Laser Filaments for Optimized Semiconductor–Metal Welding. *Laser Photonics Rev.*, 15(2):2000433, 2021.
143. J.H. Marburger. Self-focusing: Theory. *Progress in Quantum Electronics*, 4:35–110, 1975.
144. H. Kämmer, G. Matthäus, K. A. Lammers, C. Vetter, M. Chambonneau, and S. Nolte. Origin of Waveguiding in Ultrashort Pulse Structured Silicon. *Laser and Photonics Rev.*, 13:1800268, 2019.
145. P. A. Temple and C. E. Hathaway. Multiphonon Raman Spectrum of Silicon. *Phys. Rev. B*, 7(8):3685–3697, 1973.
146. J. Bonse, K. W. Brzezinka, and A. J. Meixner. Modifying single-crystalline silicon by femtosecond laser pulses: An analysis by micro Raman spectroscopy, scanning laser microscopy and atomic force microscopy. *Appl. Surf. Sci.*, 221(1-4):215–230, 2004.
147. S. F. Preble, Q. Xu, B. S. Schmidt, and M. Lipson. Ultrafast all-optical modulation on a silicon chip. *Opt. Lett.*, 30(21):2891–2893, 2005.
148. V. R. Almeida, C. A. Barrios, R. R. Panepucci, and M. Lipson. All-optical control of light on a silicon chip. *Nature*, 431:1081–1084, 2004.
149. F.C. Ndi, J. Toulouse, T. Hodson, and D. W Prather. All-optical switching in silicon photonic crystal waveguides by use of the plasma dispersion effect. *Opt. Lett.*, 30(17):2254–2256, 2005.
150. Ö. Boyraz, P. Koonath, V. Raghunathan, and B. Jalali. All optical switching and continuum generation in silicon waveguides. *Opt. Express*, 12(17):4094–4102, 2004.
151. M. Schultze, E. M. Bothschafter, A. Sommer, S. Holzner, W. Schweinberger, M. Fiess, M. Hofstetter, R. Kienberger, V. Apalkov, V. S. Yakovlev, M. Stockman, and F. Krausz. Controlling dielectrics with the electric field of light. *Nature*, 493(7430):75–8, 2013.
152. Ferenc Krausz and Mark I. Stockman. Attosecond metrology: from electron capture to future signal processing. *Nat. Photonics*, 8(3):205–213, 2014.
153. M. Schultze, K. Ramasesha, C. D. Pemmaraju, S. A. Sato, D. Whitmore, A. Gandman, J. S. Prell, L. J. Borja, D. Prendergast, K. Yabana, D. M. Neumark, and S. R. Leone. Attosecond band-gap dynamics in silicon. *Science*, 346(6215):1348–1352, 2014.
154. R. van Erp, R. Soleimanzadeh, L. Nela, G. Kampitsis, and E. Matioli. Co-designing electronics with microfluidics for more sustainable cooling. *Nature*, 585(7824):211–216, 2020.
155. A. Mouskeftaras, S. Beurthey, J. Cogan, G. Hallewell, O. Leroy, D. Grojo, and M. Perrin-Terrin. Short-pulse laser-assisted fabrication of a si-sio$_2$ microcooling device. *Micromachines*, 12(9):1054, 2021.